



RESEARCH ARTICLE

10.1029/2020JG005960

Greenhouse Gas Exchange of a NW German Peatland, 18 Years After Rewetting

Carsten Schaller¹ , Bernd Hofer², and Otto Klemm¹ 

¹University of Münster, Institute of Landscape Ecology, Climatology Research Group, Münster, Germany, ²Hofer & Pautz GbR, Altenberge, Germany

Key Points:

- First attempt to include ozone into the greenhouse gas balance of a rewetted raised bog. The deposition of ozone adds a cooling effect
- The site is still a net source of greenhouse gases
- It is likely that the yearly GHG emissions are lower than they would have been if restoration had not started 18 years ago

Correspondence to:

C. Schaller,
carsten.schaller@uni-muenster.de

Citation:

Schaller, C., Hofer, B., & Klemm, O. (2022). Greenhouse gas exchange of a NW German peatland, 18 years after rewetting. *Journal of Geophysical Research: Biogeosciences*, 127, e2020JG005960. <https://doi.org/10.1029/2020JG005960>

Received 8 JUL 2020
Accepted 19 OCT 2021

Abstract Undisturbed peatlands are usually a sink of greenhouse gases (GHG), but turn to a GHG source when drained. While rewetting and restoration of drained peatlands play an important role in efforts to mitigate global warming, high uncertainties exist concerning the time period it takes after the start of rewetting until the point when the peatland becomes a GHG net sink. We investigated a site within the “Uchter Moor”, NW Germany. It is an oligotrophic raised bog, which was never used for agriculture, but was drained in 1950 for peat mining. In 1999, restoration began; now the ecosystem is in transition back to a typical raised bog vegetation with *Eriophorum vaginatum*, *Molinia caerulea* and *Eriophorum angustifolium* being the dominant species. *Sphagnum cuspidatum* appears in patches. From June 2016 to January 2018, an eddy covariance (EC) tower measured the fluxes of carbon dioxide (CO₂), methane (CH₄), and nitrous oxide (N₂O). The flux of ozone (O₃) was also measured for 6 months by EC and modeled for the remaining experimental period. Using the sustained global warming potential for a 100-year time horizon, the balance of CO₂, CH₄, and N₂O in 2017 was +500 ± 120 g CO₂-equiv m⁻² a⁻¹. The plus sign indicates a net emission of GHG into the atmosphere. Methane contributed 78% to this flux. The inclusion of O₃ into the balance yielded a somewhat smaller total flux of +430 ± 120 g CO₂-equiv m⁻² a⁻¹. Overall, the peatland is still a source of GHG, 18 years after re-wetting.

Plain Language Summary Undisturbed peatlands usually have a long-term cooling effect on global climate. If drained, peatlands turn from a sink to a source of greenhouse gases (GHG), which leads to a long-term warming effect on climate. More recently, many drained peatlands have been re-wetted. One of the goals is to bring back the peatland from a source to a sink of GHG, and thus mitigate the human-made global warming. There is still uncertainty about how much time a peatland ecosystem requires in order to turn back to a GHG sink. We measured the exchange fluxes of GHG between peatland and the atmosphere in a restored raised bog in NW Germany, which was re-wetted 18 years earlier. In the year 2017 the restored ecosystem was still a net source of long-lived GHG (carbon dioxide, methane, nitrous oxide). When including the short-lived GHG ozone, the total balance was still positive, but ozone adds a cooling effect. We hypothesize that it will take another few decades before the peatland is a net sink of these GHG. However, in direct comparison the GHG emissions are already lower than in comparable peatlands, which were still drained for the purpose of peat extraction.

1. Introduction

Peatlands cover only 3% of the Earth's land surface, but they store about 25% of the global carbon (C) pool (Leifeld & Menichetti, 2018; Page & Baird, 2016). They play a major role in the global biogeochemical cycles (Gorham, 1991) and the Earth's climate system, because they act as sources and sinks of greenhouse gases (GHG) such as carbon dioxide (CO₂), methane (CH₄), and nitrous oxide (N₂O). Undisturbed, growing peatlands under natural conditions usually act as long-term C and GHG sinks, that is, following the first centuries to thousands years after initiation, the cooling effect of CO₂ sequestration outweighs the warming effect of short-lived CH₄ emissions (Frolking & Roulet, 2007; Mathijssen et al., 2017). In Europe, including the European part of Russia, still a fraction of 54% of the peatlands are undisturbed. Focusing on Germany, the fraction of peatlands that still accumulate peat (mires) is only ~2% (Joosten et al., 2017; Tanneberger et al., 2017). The high percentage of degraded peatlands in Germany and other areas of western Europe puts these ecosystems into the focus of global climate research. When peatlands are drained, this leads to peat oxidation and mineralization and turns peatland ecosystems from a net sink to a net source of GHG (Blodau, 2002; Blodau et al., 2004; Joosten, 2010; Leifeld & Menichetti, 2018; Page & Baird, 2016). The contributions of agriculture, forestry, and peat mining to peatland losses are estimated to be 50%, 30%, and 10%, respectively (Joosten & Clarke, 2002). After the termination of

© 2022. The Authors.

This is an open access article under the terms of the [Creative Commons Attribution License](https://creativecommons.org/licenses/by/4.0/), which permits use, distribution and reproduction in any medium, provided the original work is properly cited.

peat mining in a given area, no vegetation is left at the abandoned peatland, which further emits CO₂ (Waddington et al., 2010; Wilson, Farrell, et al., 2016).

To date, peat has been cut over an area of more than 300 km² (Speyer, 2012) in NW Germany. Since the 1980s, abandoned cutover peatlands must, by law, be rewetted for the purpose of nature restoration (Höper et al., 2008; Speyer, 2012) and climate change mitigation (Leifeld & Menichetti, 2018). Rewetting is also the general global warming mitigation measure for degraded peatlands as discussed in the IPCC guidelines for national GHG inventories (IPCC, 2014). Due to the increased water level shortly after rewetting, the emissions of CO₂ (Komulainen et al., 1999; Tuittila et al., 1999) as well as of N₂O (Alm et al., 2007) may decrease. Synchronously, the emissions of CH₄ may increase due to a lower CH₄ oxidation and enhanced methanogenesis (Augustin & Joosten, 2007; Komulainen et al., 1998; Tuittila et al., 2000). In the following years to several decades, CH₄ emissions are expected to decrease, eventually turning the ecosystem back to a net GHG sink (Augustin & Joosten, 2007).

Over the past years, very good understanding on the relevant biogeochemical processes in restored peatlands has been developed (Andersen et al., 2017; Bacon et al., 2017). However, high uncertainties still exist, concerning the time period it takes after the start of rewetting until the point when the peatland becomes a GHG net sink. Some authors report a quite rapid decrease of GHG emissions within a few years after rewetting (e.g., Kivimäki et al., 2007; Tuittila et al., 1999; Wilson et al., 2013), while others report still high GHG emissions up to decades after rewetting (e.g., Vanselow-Algan et al., 2015; Wilson et al., 2009, 2007). The causes for these very diverse results are different conditions in land-use before and after rewetting including fertilization (e.g., Harpenslager et al., 2015; Kandel et al., 2019), vegetation composition (e.g., Huth et al., 2021; Putkinen et al., 2018), soil biogeochemistry (e.g., Andersen et al., 2006; Emsens et al., 2020; Huth et al., 2021), water level fluctuations (e.g., Järveoja et al., 2016; Zhong et al., 2020), and local climate (e.g., Nijp et al., 2015; Teklemariam et al., 2010). Overall though, the available data on GHG fluxes from rewetted peatlands and the understanding of the change of these fluxes over time is still limited (Bacon et al., 2017). Thus, this study aims to add new information on the flux balance of CO₂, CH₄, and N₂O, for a representative NW German cutover raised bog, 18 years after rewetting.

CO₂, CH₄, and N₂O are the most commonly investigated GHG in peatland restoration studies. They can be viewed as the drivers of peatlands' anthropogenic greenhouse effect, because the respective exchange fluxes of these gases between peat and the atmosphere are a direct result of the human-made rewetting process after drainage. However, tropospheric ozone (O₃) is an important GHG as well. It is not emitted directly by ecosystems or human-made processes. It is a secondary pollutant, produced photochemically from NO₂ and oxidation of carbon monoxide (CO), CH₄, and non-CH₄ volatile organic compounds (NMVOC; Myhre et al., 2013). Since pre-industrial times, the concentration of these O₃ precursors have been rising dramatically (Lamarque et al., 2010), and, as a consequence, the tropospheric O₃ concentration has substantially increased as well (Monks et al., 2015; Myhre et al., 2013). This makes tropospheric O₃ a strong anthropogenic greenhouse gas and the third most important contributor to global radiative forcing (Myhre et al., 2013). Since oligotrophic raised bogs usually do not emit NO_x, it is, in our case, the background O₃ which is advected by the wind and deposited to the peatland through turbulent motion. The peatland thus acts as a strong sink of near-surface O₃ (Galbally & Roy, 1980; M. L. Wesely & Hicks, 2000). Ozone gets deposited at the surface of water and soil, where it is decomposed rapidly (Lamaud et al., 2009; Stella, Personne, et al., 2011). Further, O₃ can be deposited on the vegetation's surface but it can also directly enter the stomata, leading to physiological damage (Guidi et al., 2001; Lamaud et al., 2009). Due to its high reactivity, tropospheric O₃ has a very short and highly variable lifetime, which depends on the location: its lifetime ranges from a few hours in NO_x polluted cities to a couple of weeks in the free troposphere (Dentener et al., 2010; Goldberg et al., 2015; Jacob, 2000; Young et al., 2013). The high lifetime variability, but also its heterogeneous spatial distribution in the atmosphere, substantially hampers the estimation of the GWP of O₃, which makes it difficult to consider O₃ in a total GHG balance. To our knowledge, no studies have yet addressed the annual O₃ flux over a rewetted raised bog ecosystem, as well as its impact on the total GHG balance.

Additionally, water vapor (H₂O) is by far the largest contributor to the greenhouse effect in the natural atmosphere (Myhre et al., 2013; Schmidt et al., 2010). Attempts addressing the global warming impact of H₂O exchange in peatlands exist, for example, addressing local evaporative cooling effects (Helbig et al., 2020). However, due to the specific properties of H₂O in the atmosphere, it is still challenging to develop measures in terms of CO₂-equivalents (e.g., Sherwood et al., 2018). We therefore decided to not include H₂O in the balance. By then including CO₂, CH₄, N₂O, and O₃, this study covers most relevant GHG for peatland ecosystems (Bacon et al., 2017; Myhre

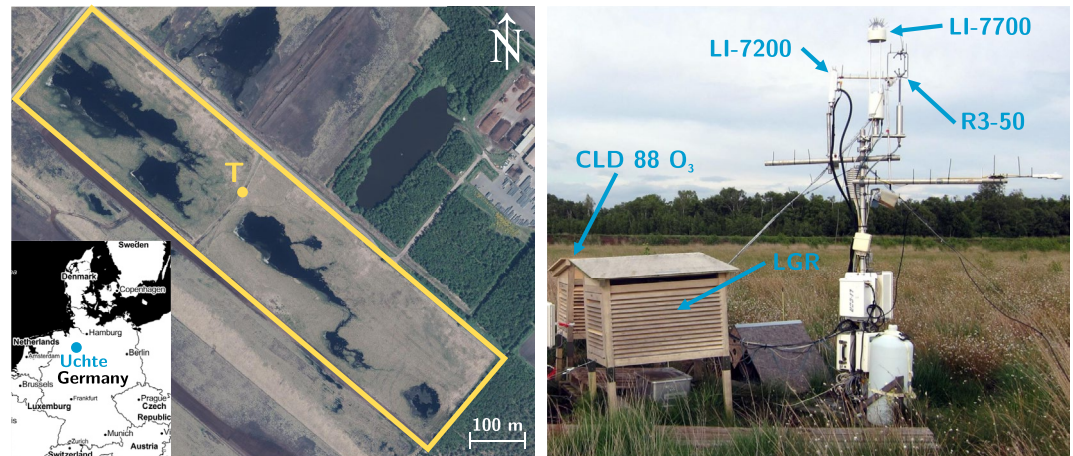


Figure 1. Left panel: Aerial image of the study area in early summer 2017. The yellow framed area denotes the actual rewetted study site, where the measurement tower (yellow “T”) was located (excerpt from “Geobasisdaten” of the Landesamt für Geoinformation und Landesvermessung Niedersachsen, Hannover, Germany, © 2019 LGLN). The map in the bottom left border locates Uchte within Germany (modified from last access: 07 May 2019, © Stamen and OpenStreetMap contributors under Creative Commons License CC-BY-SA). Right panel: EC tower equipped with all measuring devices in June 2017. The closed path analyzers were located in wooden weather huts, while the rain gauge was situated behind the photographer. Line of sight is northeast.

et al., 2013). Thus, this paper provides a first attempt of a complete assessment of the total annual GHG balance of a NW German raised bog, 18 years after rewetting.

2. Material and Methods

2.1. Study Site

The study site (Figure 1, left) is located within the “Uchter Moor”, about 6 km west of the township Uchte, NW Germany. It is part of the Ramsar wetland area “Diepholzer Moorniederung” (Ramsar Sites Information Service, 1976). It extends over 5,660 ha, of which 3,263 ha are under high-priority nature protection (BUND Diepholzer Moorniederung, 2016). The onset of peat growth is estimated at about 7,000–7,500 years ago, that is, during the early Atlantic period of the Holocene (Schneekloth & Schneider, 1970). Peat was cut manually from 1930 on; from 1955 on, the cutting process was switched to industrial peat mining (Richard, 1990), which has been in operation up to today.

The actual study site (52° 30′ 30″ N, 8° 49′ 33″ E, 40 m above sea level, site code DE-UtM in the European Fluxes Database Cluster) is a raised bog that remained completely undisturbed until 1950. At that time, it was drained and the peat was cut using industrial machinery until 1998. Overall, up to 2–3 m peat was cut and 0.5 m of peat was left undisturbed. In 1999, restoration started by constructing dams, filling up of the cut-over areas with *Bunkerde*, and rewetting within an area that is about 19 ha. *Bunkerde* is the upper original rooted soil layer with vegetation, which was removed from the site before cutting the peat and stored for the later restoration (Money & Wheeler, 1999). A continuous vegetation monitoring of the site since the beginning of the rewetting revealed an increasing abundance of *Sphagnum cuspidatum* patches from 1999 until 2006. Since then, the increase of *Sphagnum cuspidatum* coverage has slowed down. The ecosystem is in transition back to a typical raised bog vegetation with *Eriophorum vaginatum*, *Molinia caerulea* and *Eriophorum angustifolium* being the dominant species. Agriculture has never been performed within the flux footprint area around the experimental site (Section 3.2), thus the bog is still in an oligotrophic state with a surface peat C/N ratio of ~50 (S. Agethen & K.-H. Knorr, personal communication, 2016).

A comparison of the O₃ concentration measured at the site and the O₃ concentration at background air quality stations outside the peatlands, about 40–80 km away, revealed a very good agreement of the O₃ levels (see Section 2.5.2). Thus, it is extremely unlikely that the site is a relevant local source of O₃ after photochemical reactions

Table 1
Mounting Distances of the Gas Analyzer Intakes on the Eddy Covariance Tower in cm, Relative to the Center of the Sonic Anemometer

Analyzer	Vertical	North	East
LI-7200	−8	6	−8
LI-7700	0	20	−5
LGR 913–1054	−15	5	−1
CLD 88 O ₃	−16	6	−2

with freshly emitted NO_x and VOC. The O₃ concentration at the site reflects the background O₃, which is moved by wind and turbulent motion to the ecosystem.

The climate is warm-temperate and fully humid with a warm summer following the Köppen-Geiger classification (Kottek et al., 2006). During the climate normal reference period 1981–2010, the long-term mean annual temperature and precipitation sum was 9.6°C and 703 mm, respectively (German Meteorological Service, weather station Rahden-Kleinendorf, 17 km southwest of the study site).

2.2. Instrumentation

An eddy covariance (EC) tower was installed from June 2016 to January 2018 and equipped (Figure 1 right) with an R3-50 sonic anemometer (Gill Instruments Ltd., Lymington, UK) at an observation height of 3.2 m above ground. We installed a LI-7700 open-path CH₄ analyzer and a LI-7200 enclosed-path CO₂/H₂O analyzer (both LI-COR Inc., Lincoln, NE, USA). The LI-7200 intake tube was 0.5 m long and had an inner diameter of 5.3 mm. Further, we employed a CH₄/N₂O/H₂O closed path analyzer LGR 913–1054 (Los Gatos Research Inc., San Jose, CA, USA), equipped with a Teflon tube (inner diameter 4.0 mm, length 4.0 m) as intake and a dry scroll vacuum pump XDS 35i (Edwards Ltd., Burgess Hill, UK). From 6 June 2017 on, we added a CLD 88 O₃ closed path analyzer (ECO PHYSICS AG, Dürnten, Switzerland) to the setup and operated it using an insulated Teflon tube of 3.9 m length and an inner diameter of 1.6 mm as inlet line. Table 1 provides details on the intake distances of all analyzers relative to the sonic anemometer. All instruments described so far were running at a data acquisition frequency of 10 Hz.

Ancillary meteorological data was measured at 0.2 Hz and aggregated to 10-min values. Data was collected for air temperature and relative humidity (HC2S3, Campbell Scientific Ltd., Logan, UT, USA, at a height of 2 m a.g.l.), barometric pressure (Model 278, Setra Systems Inc., Boxborough, MA, USA) as well as shortwave and longwave radiation in both upwelling and downwelling directions using a CNR4 net radiometer (Kipp & Zonen B.V., Delft, The Netherlands). Soil temperature was measured in a depth of −5 cm below ground level using a Pt100 resistance thermometer (WK63, UGT GmbH, Müncheberg, Germany). A heated tipping bucket rain gauge 52202 (R.M. Young Company, Traverse City, MI, USA) measured precipitation, while heating was switched on only for air temperatures $T_a < 1^\circ\text{C}$. All measurements described so far, including EC, were logged centrally using a CR3000 micrologger (Campbell Scientific Ltd., Logan, UT, USA). The water level of the bog ecosystem relative to the ground surface was measured using a standalone diver DI272 (Van Essen Instruments B.V., Delft, The Netherlands), which has an integrated data logger. To detect the existence of snow cover during the winter season, pictures of a webcam were stored every 10 min and evaluated manually. The timestamps of all collected datasets refer to Central European Time (CET/UTC + 1 hr) throughout the whole measuring period.

2.3. Raw Data Processing and Flux Calculation

Half-hourly fluxes of H₂O, CO₂, CH₄, N₂O, O₃ were calculated from the high-frequency data using the proved processing routine (Fratini & Mauder, 2014) of the software package EddyPro v6.2.2 (LI-COR Inc., Lincoln, NE, USA). The EddyPro routine included despiking (MAD test, Mauder et al., 2013), double coordinate rotation into the mean wind field (Kaimal & Finnigan, 1994; Aubinet et al., 2000), Reynolds decomposition of turbulent fluctuations by block averaging, covariance maximizing and spectral corrections in the high-frequency (Ibrom, Dellwik, Flyvbjerg, et al., 2007) and low-frequency range (Moncrieff et al., 2004). For CH₄ data from the LI-7700, fluctuations in air density were considered (McDermitt et al., 2011; Webb et al., 1980). The CLD 88 O₃ does not measure water vapor, therefore dilution effects of the O₃ mole fraction were corrected (Ibrom, Dellwik, Larsen, & Pilegaard, 2007). Data from LI-7200 and LGR 913–1054 were already available as mixing ratio. To obtain highly reliable results, raw data were discarded if the relative signal strength indicator (RSSI) of the LI-7200 was <80%. For the LI-7700, the respective threshold was set to RSSI <20%. Raw data of LGR 913–1054 and CLD 88 O₃ were discarded in case of anomalies of the optical cell temperature, pressure readings and device malfunctions. All data work besides the EddyPro processing was performed using *R* (R Core Team, 2017). Using the half-hourly EC results, the flux footprint over the whole measuring period was calculated after (Kljun et al., 2015). The

high-frequency cospectra (Kaimal et al., 1972; Kaimal & Finnigan, 1994) were checked for disturbed turbulence flow induced by the wooden weather huts (Figure 1) and no signs for flow distortion effects were found.

2.4. Quality Assurance and Gap-Filling

To fulfill the EC assumptions of steady state conditions and well developed turbulence, we applied the overall quality flag policy of Foken et al. (2004), which is based on 9 quality grades from “0” (best) to “9” (poorest). Only half-hourly data with flags ≤ 6 were kept. To ensure that flux calculation and quality flagging performed as expected, the remaining data was additionally checked visually. Here, some unreasonably high negative and positive CO_2 fluxes were detected. These were discarded by calculating a running 95% quantile of the absolute flux random uncertainty estimate (RUE, Finkelstein & Sims, 2001) over a centered running time window having a 14-day duration. Fluxes, for which the associated RUE was outside the 95% quantile were removed. All flagged data were excluded from further analysis. After that procedure, there were gaps of 20% for sensible heat flux H , 27% for latent heat flux LE (LI-7200), 27% for H_2O flux $F_{\text{H}_2\text{O}}$ (LI-7200), 27% for CO_2 flux F_{CO_2} , 14% for N_2O flux $F_{\text{N}_2\text{O}}$, 15% for CH_4 flux $F_{\text{CH}_4}^{\text{LGR}}$, and 62% for CH_4 flux $F_{\text{CH}_4}^{\text{LI77}}$ of the time series. By combining the quality-checked flux data from the two CH_4 analyzers, $F_{\text{CH}_4}^{\text{LI77}}$ and $F_{\text{CH}_4}^{\text{LGR}}$, the percentage of gaps for F_{CH_4} decreased to 12%. To ensure that the fluxes resulting from the two CH_4 analyzers are comparable, an orthogonal regression analysis was conducted. With slope $m = 0.91$, intercept $t = 0.00$, Spearman's $\rho = 0.94$ and the root mean square error $\text{RMSE} = 12 \text{ nmol m}^{-2} \text{ s}^{-1}$, a very good agreement between $F_{\text{CH}_4}^{\text{LI77}}$ and $F_{\text{CH}_4}^{\text{LGR}}$ was found. This agreement is in accordance with, but slightly is better than reported by Detto et al. (2011) for a similar setup of an LI-7700 and an LGR fast greenhouse gas analyzer (FGGA), which is based on the same spectroscopy technology as the 913–1054. Taking the entire measuring period into account, the percentage of gaps is still in a similar order of magnitude. For the measured O_3 flux, $F_{\text{O}_3}^{\text{EC}}$, 15% of data between 6 June and 31 December 2017 are missing.

For cumulative flux calculations and annual balances, a gap-free data set is necessary. Due to power outages or device failures, some of the gaps are present not only in the flux data but also in the ancillary meteorological measurements. However, these ancillary data are absolutely required for the gapfilling of the fluxes as well as for the calculation of the synthetic ozone flux (Section 2.5). To provide a reliable, gap-free timeseries, the missing data was downloaded from the German Meteorological Service (DWD) homepage (<ftp://opendata.dwd.de/>) as half-hourly data for T_a , relative humidity R , and barometric pressure p from the nearest weather station Diepholz (30 km west-northwestern). For the synthetic ozone flux (Section 2.5), the hourly friction velocity (u^*) mean was also required. As u^* was not available in the Diepholz dataset, a monthwise linear regression model, based on hourly data, where u_{uchte}^* is a function of the wind speed U_{Diepholz} , was calculated to predict u_{uchte}^* in case of missing values. To ensure that the predicted u^* was comparable with the measured u^* , an orthogonal regression analysis on every monthly model was applied. With $m = [0.78; 0.94]$, $t = [0.02; 0.05]$, Spearman's $\rho = [0.74; 0.92]$ and $\text{RMSE} = [0.06; 0.10] \text{ m s}^{-1}$, a good agreement was found. To avoid circular reasoning, every second value of the dataset was used to fit the linear model for validation of the model only, while the other half of data was used to predict u^* .

To exclude values of F_{CO_2} being biased during nighttime, periods with low u^* were discarded following the moving point method (Papale et al., 2006). The final u^* threshold was obtained using the median result of the bootstrapping estimate (Wutzler, Lucas-Moffat, et al., 2018) with 200 replicates. Seasonal variability of the threshold was taken into account using a windowed approach, where the u^* threshold was calculated in steps of 3 months. Finally, after all quality assurance steps (flagging, RUE, u^*), 33% of F_{CO_2} had to be gapfilled.

The gaps in all flux time series except O_3 were filled using the marginal distribution sampling (MDS) approach by Reichstein et al. (2005). The MDS method combines the look-up table (LUT) approach with the mean diurnal course (MDC) approach (Falge et al., 2001). In the MDS method, first a LUT was created, where fluxes are binned in classes of similar micrometeorological conditions within a defined time window. Missing values are then replaced with the average flux for the associated class of similar meteorology. Only in cases when no meteorological data was available, the MDC method was used instead, which replaces missing values with the average value at the same hour of day within a certain moving time window. For the CH_4 flux, the vapor-pressure deficit ΔE , the water level and the soil temperature 5 cm below ground level T_s^5 was used to fill the LUT. For $F_{\text{N}_2\text{O}}$, the water level, T_s^5 and the sum of precipitation were employed. For H , LE , $F_{\text{H}_2\text{O}}$, and F_{CO_2} , we used ΔE , T_a , and the shortwave down-welling radiation $K \downarrow$ as explaining variables.

We used REddyProc v1.1.5 (Wutzler, Lucas-Moffat, et al., 2018; Wutzler, Reichstein, et al., 2018) for all u^* bootstrapping and MDS gapfilling procedures. For $F_{O_3}^{EC}$ no gapfilling routine was applied.

2.5. Synthetic Ozone Flux

Because measured ozone fluxes were available only for the second half of 2017, we used the approach by Ducker et al. (2018) to estimate a hourly synthetic ozone flux

$$F_{O_3}^{syn} = -v_d \cdot \rho_a \cdot \chi \quad (1)$$

for the entire measuring period, where ρ_a is the molecular density of air, χ the mole fraction of O_3 , and v_d denotes the deposition velocity of O_3 . A minus sign is introduced into the equation, to fulfill the micrometeorological conventions that fluxes toward the Earth's surface are always negative and, at the same time, deposition velocities associated with a negative flux are positive numbers. The inverse of v_d , v_d^{-1} can be expressed as resistances (M. Wesely, 1989; Ducker et al., 2018)

$$v_d^{-1} = r_a + r_b + (r_s^{-1} + r_{ns}^{-1})^{-1}, \quad (2)$$

where r_a denotes the aerodynamic resistance, which depends on near-surface turbulence conditions like the roughness length and u^* . The boundary layer resistance r_b considers the properties, for example, molecular diffusivity, of the gas in air, and $(r_s^{-1} + r_{ns}^{-1})^{-1}$ expresses the canopy and ground surface resistance, where the part of the ozone flux that enters the stomata corresponds to the stomatal resistance r_s . The remaining non-stomatal resistance r_{ns} describes the portion of the flux that terminates on the surfaces of ground or vegetation (Ducker et al., 2018) and its associated supplement provides information on the methodology in detail.

To obtain the synthetic O_3 flux, several input parameters were necessary. Most of them were available and used directly from the instrumentation at the study site: Displacement height, roughness length, u^* , H , LE , water vapor flux F_{H_2O} , R , T_a , p . We assumed $\left(\frac{Sc}{Pr}\right)^{\frac{2}{3}} = 1.14$ for O_3 and 0.87 for H_2O following Erisman et al. (1994), where Sc denotes the Schmidt number and Pr the Prandtl number. For the calculation of r_{ns} , we followed the parametrization by Zhang et al. (2002); Zhang et al. (2003), where the reference value for in-canopy aerodynamic resistance was set to $r_{ac0} = 20 \text{ s m}^{-1}$. The dry-cuticle uptake resistance of O_3 was assumed $r_{cutd0} = 500 \text{ s m}^{-1}$ for the land use category "swamp". The soil resistance was set to $r_g = 500 \text{ s m}^{-1}$ as recommended by Zhang et al. (2003) for wet ground. In the case of a snow cover at the site, $r_g = 2000 \text{ s m}^{-1}$ was taken instead.

2.5.1. Leaf Area Index

The leaf area index (LAI), which is necessary to calculate r_{ns} , was estimated using the Sentinel-2 Toolbox (S2TBX v6.0.3, European Space Agency, Paris, France) as part of the Sentinel Application Platform (SNAP v6.0, European Space Agency, Paris, France). Cloud-free Sentinel-2 multispectral imagery (Drusch et al., 2012) was obtained from the Copernicus Sentinel Scientific Data Hub (<https://scihub.copernicus.eu/dhus/>). If available, we directly used Sentinel-2 Level-2A data, which are already atmospheric-corrected bottom-of-atmosphere (top-of-canopy) reflectance images. Only if Level-2A data was not available, we generated Level-2A images from the associated Level-1C top-of-atmosphere reflectance images using the Sen2Cor (Louis et al., 2016) atmospheric correction processor v2.5.5 (European Space Agency, Paris, France). The Level-2A imagery has 13 spectral bands in the short-wave, near infrared and visible regions in three different spatial resolutions of 10, 20 and 60 m (Drusch et al., 2012). After resampling of the 10 m resolution bands to a resolution of 20 m, the biophysical processor tool integrated in S2TBX was applied. It calculates the LAI based on a neural network approach, which had been trained using simulations by radiative transfer models (Weiss & Baret, 2016). In a next step, only the 85 pixels located within the study site ecosystem were kept and averaged. S2TBX provides a quality flag for the LAI results and only estimates free of any error were taken into account for the averaging process. The calculated mean LAI values range from 0.3 (February 2017) to 1.9 (August 2016). As the revisit frequency of the Sentinel-2 satellites is >1 day and only cloud-free imagery could be used, there are gaps in data of lengths between 3 and 53 days. These gaps were filled by linear interpolation.

Table 2
Spearman's ρ , Slope m and Intercept t of an Orthogonal Regression Analysis Comparing Measured Against Predicted Ozone Densities

Model formula	ρ	m	t	Gaps
U ~ SO + AT + WB	0.93	1.06	0.00	10.9%
U ~ AT + WB	0.92	1.08	0.00	8.0%
U ~ SO + WB	0.92	1.08	0.00	5.5%
U ~ SO + AT	0.91	1.09	0.00	2.4%
U ~ WB	0.88	1.12	-0.01	1.5%
U ~ AT	0.88	1.12	-0.01	1.2%
U ~ SO	0.86	1.16	-0.01	*0.0%

Note. To avoid circular reasoning, every second value of the dataset was used to fit the linear model for validation only, while the other half of data was used for prediction. Models are ordered by Spearman's ρ , while the last column gives the percentage of remaining gaps after inserting the predicted values into the final timeseries. After applying the last model, one single missing value* (0.01%) was gap-filled linearly.

2.5.2. Ozone Mole Fraction

Equation 1 requires the hourly O_3 mole fraction χ . Data for χ were derived using O_3 molar density measurements from three background air quality stations of the German State of Lower Saxony ("Landesüberwachungsnetz Niedersachsen", LÜN). The respective stations, "Allertal" (AT), "Südoldenburg" (SO) and "Weserbergland" (WB) were located 65, 80, and 40 km in northeastern, northwestern, and south-southeastern directions from Uchte, respectively. Depending on the availability of O_3 data at these three sites, seven linear additive regression models were fitted to predict the concentration in Uchte, O_3^U . In the first model, O_3^U depends on 1) O_3^{AT} , O_3^{SO} and O_3^{WB} . In the second to fourth model, O_3^U depends on two variables: 2) O_3^{AT} , O_3^{WB} ; 3) O_3^{SO} , O_3^{WB} and 4) O_3^{SO} , O_3^{AT} . Models 5–7 consist of just one explaining variable O_3^{WB} , O_3^{AT} and O_3^{SO} , respectively. All models were fitted using data from 6 June 2017 to 31 December 2017, when the CLD88 O_3 analyzer was present in Uchte. Regarding the residuals, the homoscedasticity criterion was always fulfilled and the distribution was symmetric, but not Gaussian. However, the assumption of Gaussian distributed residuals is not strictly required, because in all cases the sample size ($n \geq 3,566$) was large enough to meet the central limit theorem. Finally, using O_3^{AT} , O_3^{SO} and O_3^{WB} as explaining variables, the concentration O_3^U was predicted for the entire measuring period. For this

purpose, all 7 models were necessary to obtain a gap-free final time series of O_3^U , because the LÜN data was not free of gaps due to electricity outages, analyzer malfunctions, and maintenance periods. The final O_3^U dataset was constructed by inserting first the predicted values of the model that showed the best fit (Spearman's ρ). Missing values were then filled using the next best models, which were ordered by decreasing Spearman's ρ . Table 2 lists all models, ordered by Spearman's ρ and their results, which will be addressed in detail in Section 3.4.1. The finally predicted O_3^U time series from 1 June 2016 to 31 December 2017 was completely continuous and gap free, except for one hour, which was interpolated linearly. The timeseries was converted from molar density to mole fraction χ and used to calculate $F_{O_3}^{syn}$.

2.6. Sustained Global Warming Potentials

To estimate the balance of all measured greenhouse gas fluxes, we used the sustained global warming potential (SGWP) approach (Neubauer & Megonigal, 2015, 2019). Unlike the most widely used global warming potential (GWP) it does not assume a single pulse emission (Myhre et al., 2013), but a continuous (sustained) emission over time, which is more justified for (peatland) ecosystem studies. The SGWP approach calculates inventories $M_i(t)$ of ecosystem-derived fluxes of a GHG i for every timestep $dt = 0.2$ a from $t = 0$ up to the time horizon H of interest. Multiplying $M_i(t)$ by the corresponding radiative efficiency A_i yields the instantaneous radiative forcing $RF_i(t)$ of each GHG. The $SGWP_i$ describes the relation of the cumulative radiative forcing of gas i to the cumulative radiative forcing of the reference gas, CO_2 ,

$$SGWP_i(H) = \frac{\int_0^H RF_i(t) dt}{\int_0^H RF_{CO_2}(t) dt}. \quad (3)$$

Over a time horizon of $H = 100$ years, we assumed $SGWP_{100}^{CH_4} = 45$ and $SGWP_{100}^{N_2O} = 270$ according to the sustained-emissions-scenario by (Neubauer & Megonigal, 2015, 2019). In this scenario, the flux of one GHG F_i was set at $1 \text{ kg m}^{-2} \text{ a}^{-1}$ with an atmospheric inventory of 0 kg m^{-2} at $t = 0$.

The SGWP of tropospheric O_3 was estimated as $SGWP_{100}^{O_3} = 29$ using Equation 3, where

$$RF_{O_3}(t) = A_{O_3} \cdot \left(F_{O_3} dt + \left[M_{O_3,(t-1)} \cdot \exp\left(\frac{-dt}{\tau}\right) \right] \right), \quad (4)$$

for $H = 100$ years. A radiative efficiency of $A_{O_3} = 3.33 \cdot 10^{-2} \text{ W m}^{-2} \text{ ppb}^{-1}$ (Iglesias-Suarez et al., 2018; Tuckett, 2016) and a tropospheric O_3 perturbation lifetime $\tau = 0.267 \text{ a}$ (Aamaas et al., 2013; Fuglestedt et al., 2010)

was assumed. All CO₂-equivalent-values given in this article are based on the SGWP approach. Values from other authors cited were recalculated accordingly.

2.7. Uncertainty Estimation

Errors in all final flux results were quantified using standard error propagation techniques (e.g., Taylor, 1997). For F_{CH_4} and F_{N_2O} the total relative error was estimated for each flux i as

$$\sigma_{TOT,i} = \sqrt{\sigma_{rRUE,i}^2 + \sigma_{SGWP,i}^2}, \quad (5)$$

where $\sigma_{rRUE,i}$ denotes the relative RUE due to EC sampling errors. It was determined as

$$\sigma_{rRUE,i} = \left\langle \sqrt{\left(\frac{\sigma_{RUE,i}}{F_i}\right)^2} \right\rangle, \quad (6)$$

where $\sigma_{RUE,i}$ denotes the absolute RUE (Finkelstein & Sims, 2001, from EddyPro processing) for every half hour, which was divided by its associated half-hourly flux F_i . $\sigma_{rRUE,i}$ was then obtained by taking the ⟨median⟩ value, which is expressed by the angle brackets. For F_{CO_2} we assumed $\sigma_{TOT} = \sigma_{rRUE}$ as there was no SGWP conversion.

For the synthetic ozone flux $F_{O_3}^{syn}$, the total relative error was estimated as

$$\sigma_{TOT} = \sqrt{\left(\frac{SE_m}{m}\right)^2 + \left(\frac{SE_t}{t}\right)^2 + \sigma_{GWP}^2}, \quad (7)$$

where m and t denote the slope and intercept, respectively, of the orthogonal regression between $F_{O_3}^{syn}$ and $F_{O_3}^{EC}$. The standard error of the mean SE_m and SE_t of slope m and intercept t , respectively, yields a measure of uncertainty for the synthetic flux against the real measured EC flux.

As there is no explicit uncertainty estimation of SGWP given by (Neubauer & Megonigal, 2015), we decided to use the uncertainties of the traditional GWP reported by (Myhre et al., 2013), which should be appropriate due to the close mathematical relationship between the SGWP and GWP approaches. For CH₄ and N₂O, we scaled the uncertainties of the GWP reported by (Myhre et al., 2013) from their given 90% confidence range to a 1σ (68.3%) range. Regarding $SGWP_{100}^{O_3}$, information on the uncertainty of A_{O_3} and τ were not available. Thus, we assume the uncertainty σ_{SGWP,O_3} to be on the order of the largest σ_{GWP} reported by (Myhre et al., 2013) and used in their study. As $\sigma_{GWP,CH_4} > \sigma_{GWP,N_2O}$ (Myhre et al., 2013) we assume an uncertainty of $\sigma_{SGWP,O_3} \approx \sigma_{GWP,CH_4} = 23.7\%$.

3. Results and Discussion

3.1. Meteorological Conditions

The mean annual T_a (2 m height) clearly exceeded the long-term average (1981–2010) by 0.6°C and 0.8°C in 2016 and 2017, respectively. At the nearest operational weather station Rahden, the 2016 mean temperature was 10.2°C. In 2017, at both Rahden weather station and the study site, the annual mean T_a was 10.4°C. During the study period the monthly mean ranged between 0.1°C (January 2017) and 19.0°C (July 2016). In January 2017 also the largest negative deviation of −1.8°C from the climatological mean was observed. The largest positive deviations from the climatological mean occurred in September 2016, March 2017 and September 2017, exhibiting differences of +3.3°C, +2.9°C and +2.7°C, respectively. Soil temperature T_s^5 (Figure 2, bottom panel) ranged between 0.7°C (January 2017) and 17.0°C (July 2016). During the months June–September 2016, T_s^5 was between 1.5°C (August) and 3.5°C (September) higher than the respective monthly data of 2017. From October to December though, T_s^5 was, by 0.9°C (November, December) to 1.1°C (October), colder in 2016 than it was in 2017.

The total annual precipitation in 2016 and 2017 was 629 and 621 mm, respectively, meaning that both were below the long-term average. Except for June with a total of 160 mm (92 mm more than climate mean), all months in the second half of 2016 were clearly drier than in 2017 (Figure 2, bottom panel). In January and from March–May 2017, the precipitation was substantially less than the climatological mean, while in July the sum was greater than usually. The months August–December 2017 were near the long-term average. A snow cover lasted only during

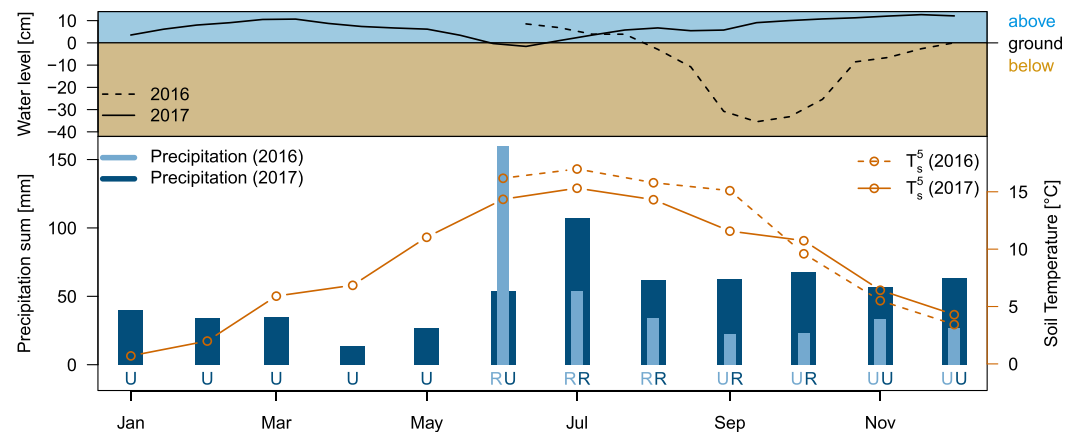


Figure 2. Upper panel: biweekly mean water level relative to the ground surface in 2016 (dashed lines) and 2017 (solid lines). Lower panel: T_s 5 cm below ground surface in 2016 (dashed lines), 2017 (solid lines) and precipitation sum (2016 in light blue, 2017 in dark blue) at the study site in Uchte (“U”). Due to power outages during thunderstorms or rain gauge failures, in some months the precipitation sum was taken from the Rahden weather station nearby, denoted as “R” below the sum bar.

the periods 13 through 19 January 2017, 8 through 11 February 2017, and on 11 December 2017. Note that Uchte data was replaced by Rahden data during months when rain gauge failures or power outages occurred.

The bog water level (Figure 2, top panel, biweekly mean) relative to ground surface in 2017 showed an annual pattern ranging from +11 cm (March) over –2 cm (July) to +13 cm (December). In contrast, 2016 data started with +9 cm in June and +7 in the first half of July, followed by a rapid decrease down to a minimum of –35 cm in late September. From that point, water level rose continuously, where ground surface was reached again in late December.

3.2. Flux Footprint

Over the entire study period, more than 85% of the measured fluxes originated from the wetland ecosystem (Figure 3). For north-northeastern to eastern and for south-southwestern to west-southwestern directions, respectively, the 90% flux contribution contour line reached somewhat over the ecosystem under study. As the main wind direction was from south western directions, a small fraction of the measured fluxes originated from the neighboring field. In this field, peat cutting had happened before, but it was not yet in the re-wetting and restoration process. We assume that the very small flux contributions from this field are statistically negligible, and the measured total fluxes are representative for the restored ecosystem of interest. During unstable stratification ($zL^{-1} < -0.2$) the footprint was constrained closer to the EC tower, so that the 90% contribution contour line for individual half-hour time periods was always well within the ecosystem. A few further exceptions occur within a small sector from north-northeastern direction. Taking the entire study period into account, there were only few cases when the wind originated from the northeast or east-northeast. The contribution of fluxes from footprint sections beyond the ecosystem under study are minor.

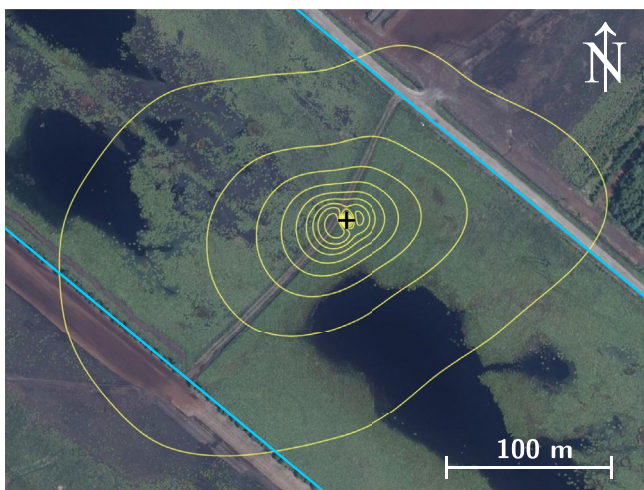


Figure 3. Aerial image of the study area in summer 2015, where the overlay shows the flux footprint based on the entire EC dataset according to Kljun et al. (2015). The yellow contour lines correspond to the 10%–90% contributions to the flux in 10% steps. The borders of the study site ecosystem are denoted by blue lines (excerpt from “Geobasisdaten” of the Landesamt für Geoinformation und Landesvermessung Niedersachsen, Hannover, Germany, © 2019 LGLN).

3.3. Comparison of CO₂, N₂O, CH₄ Fluxes Late 2016 With Those Late 2017

The months June to December were covered by measurements both in 2016 and 2017, which allows a direct comparison of these periods with each other (Figure 4). For N₂O, the monthly mean fluxes were extremely small both in

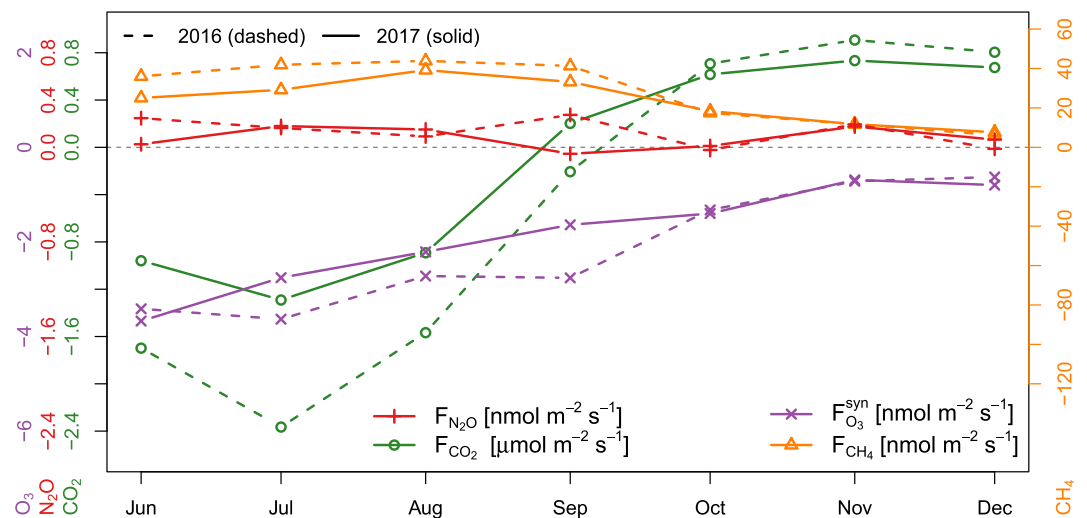


Figure 4. Mean monthly flux of CO_2 , CH_4 , N_2O (see discussion in Section 3.3), and O_3 (see discussion in Section 3.4.3) during the months June to December in 2016 (dashed lines) and 2017 (solid lines). Note the different unit magnitudes given in legend at the bottom.

2016 and 2017, ranging from $-0.05 \text{ nmol m}^{-2} \text{ s}^{-1}$ (September 2017) to $+0.27 \text{ nmol m}^{-2} \text{ s}^{-1}$ (September 2016). In the months April, June, and October 2017, F_{N_2O} was not significantly different from zero. Differences between the seasons (summer vs. winter) were not observed.

The monthly F_{CH_4} in 2016 (Figure 4, dashed orange line) started in June 2016 with $36 \text{ nmol m}^{-2} \text{ s}^{-1}$ and continuously increased up to $44 \text{ nmol m}^{-2} \text{ s}^{-1}$ in August. From then on, F_{CH_4} decreased to a minimum of $6 \text{ nmol m}^{-2} \text{ s}^{-1}$ in December. In 2017 (Figure 4, solid line), F_{CH_4} generally showed the same pattern, but the monthly flux in June to September was lower, by up to $13 \text{ nmol m}^{-2} \text{ s}^{-1}$ (July). From October to December, there was no difference between the years.

Due to photosynthetic CO_2 assimilation, the monthly F_{CO_2} in 2016 was directed toward ground from June to September, turning the ecosystem into a net sink of CO_2 and reaching a maximum flux of $-2.4 \text{ μmol m}^{-2} \text{ s}^{-1}$ in July. From October–December 2016, a positive F_{CO_2} of up to $0.9 \text{ μmol m}^{-2} \text{ s}^{-1}$ was observed. In contrast to 2016, the 2017 F_{CO_2} was only negative from June to August. The mean fluxes during these months were significantly lower than in 2016, reaching only a maximum of $-1.3 \text{ μmol m}^{-2} \text{ s}^{-1}$ (July). In September–December 2017, the ecosystem was a net source for CO_2 with mean fluxes of up to $0.7 \text{ μmol m}^{-2} \text{ s}^{-1}$, which was slightly less than it was in 2016.

To summarize here, for both CO_2 and CH_4 and the months from June to September, larger absolute fluxes were observed in 2016 as compared to 2017. For F_{CO_2} , the meteorological observations give reasons for these findings as the total sunshine duration ($K \downarrow \geq 120 \text{ W m}^{-2}$) during April, May and July–September 2016 exceeded the corresponding 2017 data by 19 (May) to 107 (September) hours. In summer 2016, more radiation led to more photosynthesis and growth. Also, the LAI in 2016 slightly exceeded the 2017 LAI by 0.2 (July) to 0.6 (September). Although the precipitation in 2016 was significantly lower (Figure 2), the water level ranged between 8 cm above ground (June) to 11 cm below ground (late August). Thus, the availability of water was not a limiting factor for the vegetation in June to August, when the greatest deviations of F_{CO_2} between the years were observed.

The small but significant difference of F_{CH_4} in June through September in 2016 as compared to the same months in 2017 might possibly be explained by T_s^5 , which was higher in 2016 than in 2017. Higher soil temperatures usually correlate with an increased microbial decay of organic matter and therefore intensify the process of methanogenesis (e.g., Inglett et al., 2012; Whalen, 2005). For the month of October, no difference of F_{CH_4} was observed between the years 2016 and 2017. This is on the one hand surprising, because differences in water level, as observed in our case (-30 cm in 2016, $+10 \text{ cm}$ in 2017), have led to considerable differences of F_{CH_4} in several other studies (e.g., Waddington & Day, 2007; Wilson et al., 2009). On the other hand, Wilson, Farrell, et al. (2016); Rinne et al. (2007); Jackowicz-Korczyński et al. (2010) reported that the F_{CH_4} did not change with

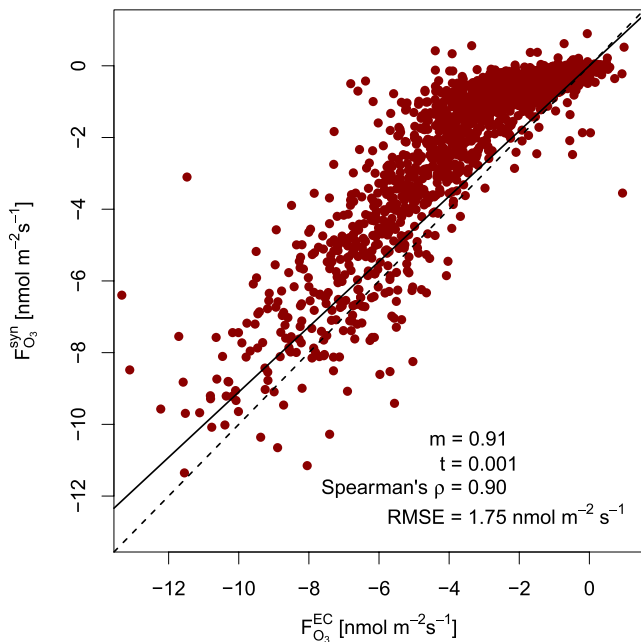


Figure 5. Synthetic ozone flux $F_{O_3}^{syn}$ against measured EC flux $F_{O_3}^{EC}$ for times with overall quality flag ≤ 6 after Foken et al. (2004) between 6 June and 31 December 2017. The solid line represents the orthogonal regression function, while the dashed line follows $f(x) = x$.

water level changes (-18 cm vs. $+20$ cm) in a restored bog with *Eriophorum angustifolium* cover. In our case, no information on the water content of the unsaturated soil layer is available. Assuming that the soil moisture content is high although the water level low, it is conceivable that no changes in F_{CH_4} were observed between the months of October in 2016 and 2017, respectively. A more detailed analysis of the processes driving the flux of CH_4 will be presented in a follow-up study.

3.4. Ozone Flux

In the following two subsections we first validate $F_{O_3}^{syn}$ against $F_{O_3}^{EC}$ to be sure that the synthetic results are reliable. Secondly, we show and discuss the typical diurnal F_{O_3} cycle.

3.4.1. Validation of Synthetic Ozone Flux

We compare the measured ozone fluxes $F_{O_3}^{EC}$ with the synthetic ozone flux $F_{O_3}^{syn}$ for the time period when both methods yield synchronous data (6 June – 31 December, 2017). To ensure that EC data met the requirements of steady-state conditions and well-developed turbulence, only time periods with overall quality flag ≤ 6 , after Foken et al. (2004), for $F_{O_3}^{EC}$ were considered. An orthogonal regression analysis (Figure 5) reveals a very good agreement of the two methods. The Spearman's correlation coefficient ρ is 0.90, intercept $t \approx 0$ and $RMSE = 1.75 \text{ nmol m}^{-2} \text{ s}^{-1}$. The slope ($m = 0.91$) is 9% less than the ideal slope of 1, that is, the synthetic ozone flux generally slightly underestimates the observed EC flux. The underestimation is larger for low fluxes, especially during nighttime, and less for higher daytime fluxes. A total of

96% of $F_{O_3}^{syn}$ values agree with $F_{O_3}^{EC}$ within a factor of 2. The observed results are reliable and agree with the methodological evaluation by Ducker et al. (2018).

3.4.2. Diurnal Ozone Flux

The EC O_3 flux exhibits a diurnal cycle with the lowest deposition fluxes happening during the night hours. For example, the median hourly flux in July 2017 (Figure 6, top panel), was $F_{O_3}^{EC} \approx -1.5 \text{ nmol m}^{-2} \text{ s}^{-1}$ between 22 and 05 hr. After sunrise, from 6:00 on, $F_{O_3}^{EC}$ continuously increased in magnitude up to $-6.9 \text{ nmol m}^{-2} \text{ s}^{-1}$ at 13:00. In the following hours, $F_{O_3}^{EC}$ remained at this flux rate until 17:00 before decreasing again until 23:00, when $F_{O_3}^{EC} = -1.5 \text{ nmol m}^{-2} \text{ s}^{-1}$. The observed O_3 flux correlated with the O_3 mixing ratio (Figure 6, bottom panel), which was lowest (≤ 20 ppb) during night time, when it decreased and reached its minimum in the early morning before sunrise. The maximum O_3 mixing ratio (40 ppb) was observed during late afternoon. Within the conceptual framework of Equation 1, the diurnal variations of the ozone deposition flux are controlled not only by the O_3 mixing ratio but also by v_d . During nighttime, $v_d < 0.1 \text{ cm s}^{-1}$ both during the cold and warm seasons. In summer, for example, in July 2017, the daytime v_d reached maxima around 0.45 cm s^{-1} (Figure 6, top panel, turquoise), supporting a higher F_{O_3} toward ground.

The observed diurnal cycles of both O_3 flux and mixing ratio can be explained by 4 primary processes: (a) near-surface O_3 mixing ratios are low during the nights. Ongoing deposition leads to a decrease of O_3 in the near-surface air. At the same time, a stable stratification and low turbulence (u^*) prevent any mixing of ozone from the residual layer during the nights. (b) With sunrise and developing turbulence, O_3 from previously decoupled layers, that is, the residual layer, is mixed downwards. (c) O_3 is produced through photochemical processing during the day. Consequently, F_{O_3} increases both due to higher O_3 mixing ratio and (d) a higher v_d triggered by developing turbulence. Due to weakening turbulence, increasing stomatal resistance and decreasing O_3 concentration, F_{O_3} decreases in the evening. Besides u^* -driven effects, the larger v_d results from daytime contribution of stomatal uptake by the vegetation (e.g., El-Madany et al., 2017; Fuhrer & Booker, 2003; Guidi et al., 2001). The observed diurnal summer O_3 flux is in very good agreement with El-Madany et al. (2017), who investigated $F_{O_3}^{EC}$ in the Mittleres Wietingsmoor, a rewetted raised bog 20 km north-northwestern from Uchte.

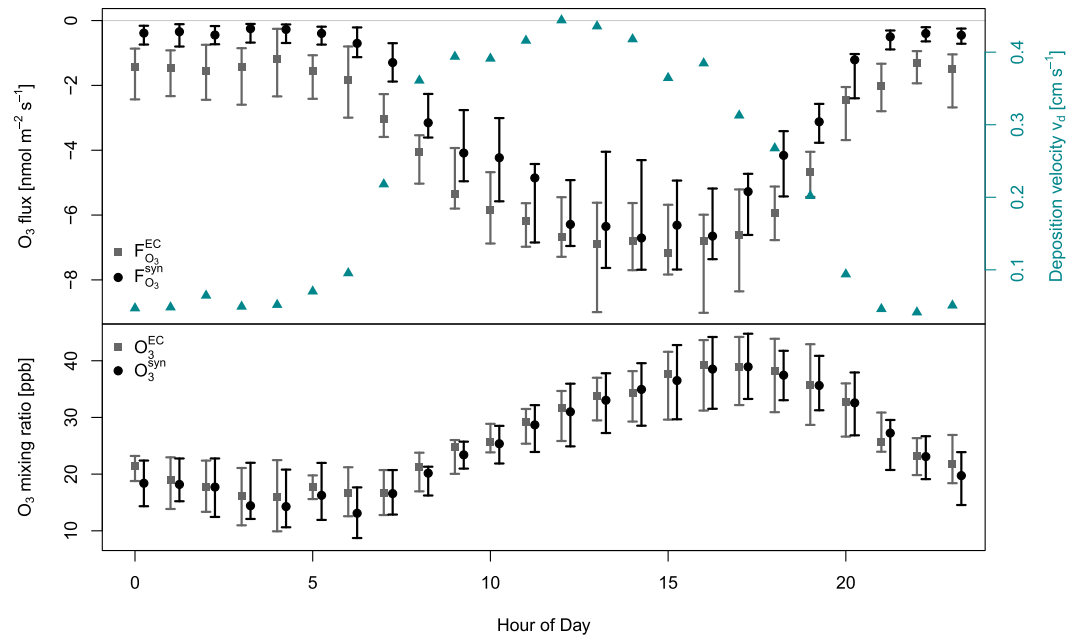


Figure 6. Top panel: median hourly $F_{O_3}^{syn}$ (black) and $F_{O_3}^{EC}$ (gray) in July 2017. The turquoise colored triangles denote the median v_d . Bottom panel: corresponding median ozone mixing ratio obtained by the Ecophysics CLD 88 O_3 (gray) and the synthetic dataset based on the regression models on the LÜN data (black). Bars denote lower and upper quartiles.

The measured and modeled ozone fluxes $F_{O_3}^{EC}$ and $F_{O_3}^{syn}$, agree well with each other. In particular, the diurnal course of the synthetic flux followed the measured flux. As mentioned in Section 3.4.1 above, $F_{O_3}^{syn}$ underestimated $F_{O_3}^{EC}$ somewhat during nighttime, when the fluxes were small. The high daytime flux toward ground was modeled very well, in this case $F_{O_3}^{syn} \approx F_{O_3}^{EC}$. Note, that $F_{O_3}^{syn}$ always used the modeled O_3 concentration based on the LÜN data, which also showed a very good agreement to the data measured in Uchte (Figure 6, bottom panel).

During the warm season, the observed diurnal variability of the O_3 flux was substantially larger than during the cold season. For example, in December 2017, both $F_{O_3}^{syn}$ and $F_{O_3}^{EC}$ did not exceed $-2 \text{ nmol m}^{-2} \text{ s}^{-1}$ during the entire day. In this month, the maximum difference between daytime and nighttime flux was only about $0.6 \text{ nmol m}^{-2} \text{ s}^{-1}$. The O_3 concentration in December 2017 was about 20 ppb without any significant variations during the day. The seasonal cycle of O_3 was not caused by fluctuations of either χ or v_d , but by a combination of both. In the winter months (December to February), both variables are small ($0.03 \leq |v_d| \leq 0.10 \text{ cm s}^{-1}$ and $\chi \leq 22 \text{ ppb}$). In the summer months (June to August) both variables reach their maxima ($0.12 \leq |v_d| \leq 0.26 \text{ cm s}^{-1}$ and $22 \leq \chi \leq 32 \text{ ppb}$) in median.

3.4.3. Comparison of the Ozone Flux Late 2016 With Late 2017

The synthetic O_3 flux was calculated both for 2016 and 2017, which allows a direct comparison of the variability of $F_{O_3}^{syn}$ between the two years. The mean monthly $F_{O_3}^{syn}$ in 2016 (Figure 4, dashed purple line) was largest in early summer with a maximum of $(-3.6 \text{ nmol m}^{-2} \text{ s}^{-1})$ in July, became lower $(-2.7 \text{ nmol m}^{-2} \text{ s}^{-1})$ in August and September, and decreased to $-0.6 \text{ nmol m}^{-2} \text{ s}^{-1}$ in December. In 2017 (Figure 4, solid purple line) the pattern was similar, but the maximum $(-3.7 \text{ nmol m}^{-2} \text{ s}^{-1})$ was already reached in June, followed by a decreasing $F_{O_3}^{syn}$ until December. In July, August, September 2017 $F_{O_3}^{syn}$ was significantly lower than in 2016. In the other months, there was no significant difference between the years.

While $F_{O_3}^{syn}$ did not differ from October to December between the two years, the results reveal a slightly larger absolute $F_{O_3}^{syn}$ in July–September 2016, compared to 2017. The two general explanatory variables of the ozone flux are v_d and χ (see previous Section 3.4.2). From June to August the monthly median χ did not show substantial differences between the two years, but in September (23 ppb in 2016, 17 ppb in 2017). The median monthly v_d was 0.25 cm s^{-1} both in June 2016 and 2017. From July to September, v_d was always by about 0.02 cm s^{-1} (September) to 0.09 cm s^{-1} (July) greater in 2016, compared to 2017. Thus, it is likely that the same reasons that led to a larger

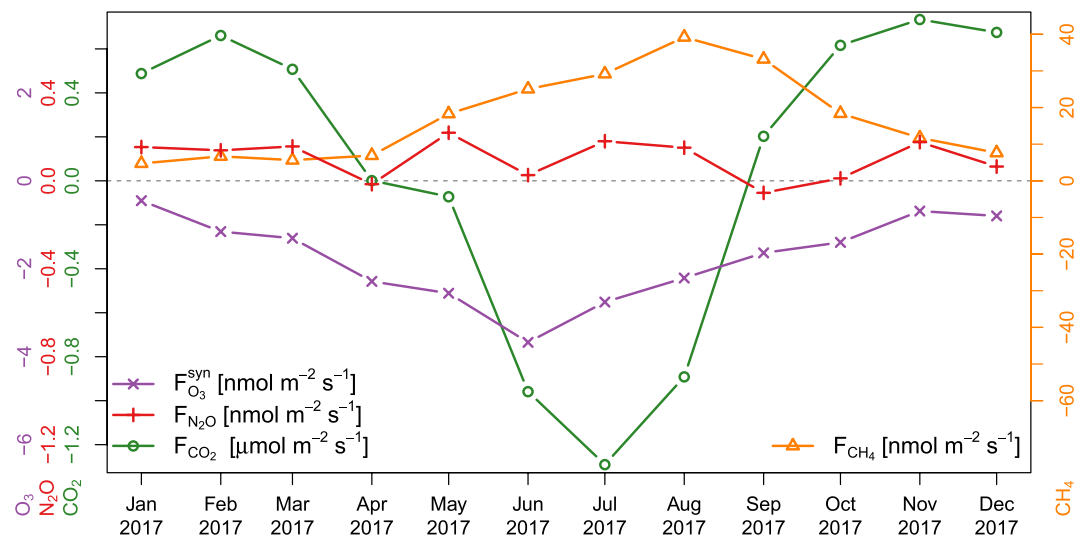


Figure 7. Monthly mean flux of the greenhouse gases in 2017. Note, that the unit magnitude and axis scaling differs between the fluxes.

F_{CO_2} (as discussed in Section 3.3) were responsible for the larger v_d and therefore a larger absolute $F_{O_3}^{syn}$. Higher photosynthetic rates likely led to a larger stomatal uptake of O_3 in 2016 as compared to 2017. In September 2016 the absolute $F_{O_3}^{syn}$ was also larger than in 2017, although the difference in v_d between the two years was quite small. In this case, the $\Delta\chi = +6$ ppb in 2016, compared to 2017, could explain the larger absolute $F_{O_3}^{syn}$.

3.5. Yearly GHG Flux Pattern in 2017

The availability of GHG flux measurements for the entire year 2017 allows a description and discussion of their seasonal cycle (Figure 7). F_{N_2O} was very low and ranged from -0.05 to $+0.22$ nmol m⁻² s⁻¹ during the entire year, independent of the season. In the months April, June, and October 2017 F_{N_2O} was not significantly different from zero. F_{CO_2} was positive from January to April and September to December with values up to 0.73 μmol m⁻² s⁻¹ in November. During these months, the net ecosystem exchange was primarily driven by respiration. Due to primary production (photosynthesis) as major driver, F_{CO_2} was directed toward the ecosystem from May to August and reached a maximum negative mean flux of -1.3 μmol m⁻² s⁻¹ in July. F_{CH_4} was always positive with a monthly mean around 6 μmol m⁻² s⁻¹ from January to April. From May, F_{CH_4} continuously increased up to 39 μmol m⁻² s⁻¹ in August. From then on, F_{CH_4} continuously decreased to 8 μmol m⁻² s⁻¹ in December. The yearly F_{O_3} cycle started with -0.5 nmol m⁻² s⁻¹ in January, reached its absolute maximum of -3.7 nmol m⁻² s⁻¹ in June, and then declined to -0.8 nmol m⁻² s⁻¹ in December.

3.6. Climate Budget for 2017

The main focus of this study was on the global warming balance of the rewetted bog ecosystem. First, we show and discuss the widely used standard balance, which includes CO_2 , CH_4 and N_2O . In the second subsection we add O_3 .

3.6.1. Standard Balance: CO_2 , CH_4 , N_2O

In 2017, the accumulated fluxes of each CH_4 , N_2O , but also CO_2 , reached a positive yearly sum (Figure 8). The positive CO_2 balance of $+72 \pm 9$ g CO_2 m⁻² a⁻¹ shows that the ecosystem respiration turned out to be stronger than the sequestration of C by photosynthesis. The annual total contribution of F_{N_2O} was $+89 \pm 33$ mg N_2O -N m⁻² a⁻¹, which equals $+38 \pm 16$ g CO_2 -equiv m⁻² a⁻¹. While F_{N_2O} contributes less to the total balance, the greatest emission of CO_2 -equiv was caused by $F_{CH_4} = +6.5 \pm 1.3$ g CH_4 -C m⁻² a⁻¹, which equals $+390 \pm 120$ g CO_2 -equiv m⁻² a⁻¹. Considering the contributions of CH_4 (78%), CO_2 (14%), and N_2O (8%), the total annual balance in 2017 summed up to $+500 \pm 120$ g CO_2 -equiv m⁻² a⁻¹.

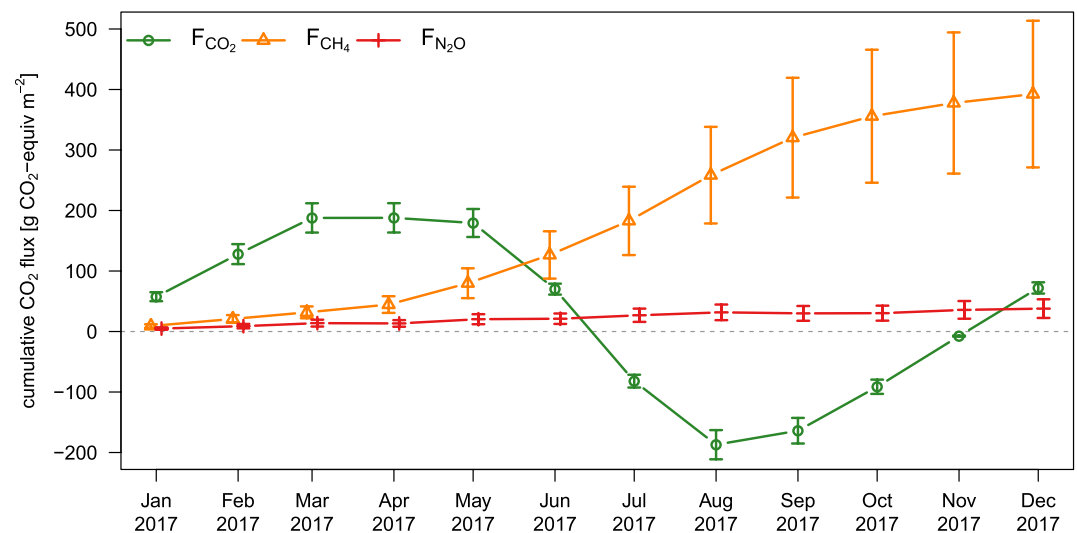


Figure 8. Cumulative balance of CO₂, CH₄ and N₂O fluxes, expressed in g CO₂-equiv m⁻². The uncertainty (see Section 2.7) is denoted by error bars.

The balance clearly revealed that 18 years after rewetting, the study site still acted as net source of CO₂-equiv. of the “standard” greenhouse gases. The site is, to a large extent, dominated by CH₄. This is in accordance with the first phase of the 3-phases-after-reflooding concept suggested by Augustin and Joosten (2007): in the first years after rewetting, F_{CO₂} generally decreases (e.g., Tuittila et al., 1999; Waddington et al., 2010), while F_{CH₄} generally increases (e.g., Waddington & Day, 2007). F_{N₂O} is in the same time most likely to decrease rapidly (e.g., Wilson et al., 2013). During this first phase, the rewetted ecosystem might be populated by aerenchymatous tissue plant species like *Eriophorum spp.*, *Molinia caerulea* (e.g., Waddington & Day, 2007) as was also the case in our study site at Uchte. These plants are known to provide an important pathway for CH₄ release under anoxic soil conditions, where the plants directly act as a CH₄ conduit (Gray et al., 2013; Greenup et al., 2000; Ström et al., 2005). A recent study from Ireland confirmed comparatively high CH₄ emissions (+14 g CH₄-C m⁻² a⁻¹, 6 years after rewetting) for a restored raised bog ecosystem dominated by *Eriophorum angustifolium* (Swenson et al., 2019). Jordan et al. (2016) also observed a higher F_{CH₄} for sites covered by *Eriophorum spp.* in comparison to sites with less aerenchymatous tissue plant species in a formerly peat extracted fen (Sweden) at soil surface water level, 15 years after rewetting. Brummell et al. (2017) found a smaller or even negative F_{N₂O} during summer at a comparable rewetted bog with a high cover of vascular plants. This effect may additionally suppress the release of N₂O at our study site. In the overall context, we suggest that our study site is currently, 18 years after rewetting, still in the first phase according to Augustin and Joosten (2007).

We hypothesize that the use of *Bunkerde* (Section 2.1) for filling up the site before rewetting also might enhance CH₄ emissions. As *Bunkerde* was the former bog surface layer including vegetation and peat, it was exposed to oxygen before rewetting. Thus, the decay process of plant matter in this soil layer was already initiated, which might enhance the decomposition of organic matter by methanogenesis after rewetting. Additionally, the *Bunkerde* introduced new labile organic matter as a major food source for methanogens into the ground. Even though we cannot prove this hypothesis, Cooper et al. (2014), and Vanselow-Algan et al. (2015) also observed higher CH₄ emissions from peatlands that had been filled with partly decayed plant matter before rewetting. We assume that similar processes occur at our Uchte study site.

The second phase after reflooding (Augustin & Joosten, 2007) is characterized by a change in plant species, with a decreasing percentage of aerenchymatous vegetation and increasing percentage of mosses (*Sphagnum spp.*), as well as other primary peatland species (Augustin & Joosten, 2007; Bain et al., 2011). In this phase, emissions of CH₄ strongly decrease, likely turning the ecosystem into a GHG sink or at least leading to a zero GHG balance. The current state of our site with *Sphagnum cuspidatum* appearing in patches and *Eriophorum vaginatum* as primary pioneer species is already a positive sign: based on practical experience from other NW German peatlands we know that the occurrence and spread of hummock-forming *Sphagnum* species could be expected about 30–40 years

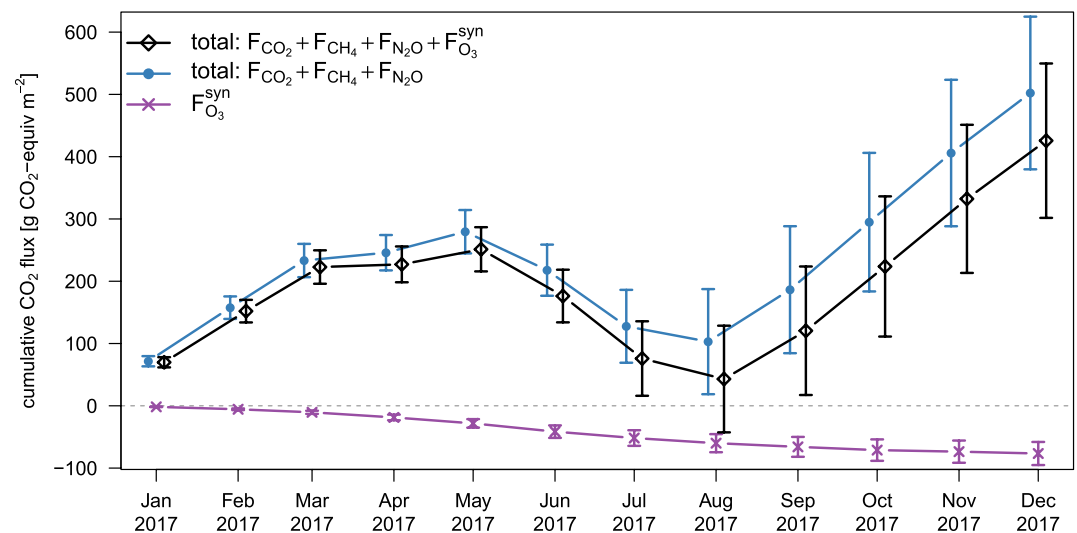


Figure 9. Cumulative balance of the O_3 flux (purple), which has a cooling effect on the total cumulative GHG balance (black) over a SGWP time horizon of 100 years. Without considering the cooling effect of O_3 , the total cumulative GHG balance would be higher (blue). All values are expressed in $g\ CO_2\text{-equiv}\ m^{-2}$. The uncertainty (see Section 2.7) is denoted by error bars.

after rewetting. Based on that finding it might be hypothesized that the study site will turn to the second phase after Augustin and Joosten (2007) within the next two decades. Note that, with the current knowledge, any kind of prediction remains difficult if not speculative. For N/NW German raised bog peat extraction sites, 30 years after rewetting, two studies resulted in a large range of observed GHG balances: (a) for two subsequent years at a site dominated by *Eriophorum angustifolium*, *Molinia caerulea*, and *Sphagnum cuspidatum*, Beyer and Höper (2015) observed an annual balance of $+0.25 \pm 0.48\ kg\ CO_2\text{-equiv}\ m^{-2}\ a^{-1}$ in 2010 and $+1.23 \pm 0.45\ kg\ CO_2\text{-equiv}\ m^{-2}\ a^{-1}$ in 2011. (b) In another restored bog in N Germany, for three restoration sites with different dominating vegetations (ericaceous shrubs, *Sphagnum spp.*, *Molinia caerulea*) and different water levels, Vanselow-Algan et al. (2015) reported extremely high balances of minimum $+3.2 \pm 0.7\ kg\ CO_2\text{-equiv}\ m^{-2}\ a^{-1}$, where CH_4 contributed $>89\%$ to the total balance. Compared to these high balances, our study site has a substantially lower warming impact on climate.

The comparison of these results with ours leads to two key findings: (a) the emissions from the Uchte site seem to be within the typical range for this kind of rewetted raised bog (Beyer & Höper, 2015) in its first phase of rewetting. (b) We observed emissions of CH_4 that may have been partly caused by the input of *Bunkerde* into the site before re-wetting. However, the CH_4 emissions are much less than those observed by Vanselow-Algan et al. (2015) at a similar site after application of *Bunkerde*.

To address the current yearly net impact of the performed land use change on global warming, we compare the net GHG balance of our restored site with that of a reference site that has not undergone any restoration so far. As there is no reference flux data available from our site before the restoration started, we use the (IPCC, 2014) emission factors, which were recently updated by (Wilson, Blain, & Couwenberg, 2016). Accepting that a temperate peatland drained for peat extraction has an emission factor (CO_2 , CH_4 , N_2O , converted from GWP to SGWP) of $+1.2\ kg\ CO_2\text{-equiv}\ m^{-2}\ a^{-1}$ as reference, our site emitted less GHG by $0.7\ kg\ CO_2\text{-equiv}\ m^{-2}\ a^{-1}$. This finding implies that due to the restoration process the yearly GHG emissions are lower than they would have been if restoration had not started 18 years ago.

3.6.2. Extended Balance Including O_3

The total 2017 O_3 flux summed up to $F_{O_3}^{syn} = -2.6 \pm 0.3\ g\ O_3\ m^{-2}\ a^{-1}$, which equals $-77 \pm 19\ g\ CO_2\text{-equiv}\ m^{-2}\ a^{-1}$ (Figure 9). Thus the annual O_3 balance has a cooling effect on the total GHG balance over a GWP time horizon of 100 years. Summing up over all GHG (CO_2 , CH_4 , N_2O , O_3) yields a total 2017 balance of $+430 \pm 120\ g\ CO_2\text{-equiv}\ m^{-2}\ a^{-1}$.

As we found in Section 3.4.2 that nighttime O₃ fluxes were slightly underestimated, the annual O₃ balance could thus be slightly higher than estimated here. However, this does not change the overall finding that the restored cut-over raised bog is still a net source of GHG in terms of CO₂-equivalents. The cooling effect of the O₃ deposition flux has an impact on the GHG balance based on the SGWP metric. For extreme short-lived climate forcers, like O₃, the SGWP metrics has shortcomings to be considered. It assumes a global distribution of the GHG being uniform or varying only moderately (Pierrehumbert, 2014). This assumption is fulfilled for GHG like CO₂, or N₂O, whose lifetimes are much longer than the mixing time of the atmosphere. Due to their very short lifetimes, short-lived climate forcers (SLCF) such as O₃ are usually not well mixed, which weakens the reliability of the estimates of their long-term radiative forcing and SGWP values (Pierrehumbert, 2014).

Due to the uncertainty introduced by the methodological shortcomings of accounting for the warming impact of O₃ as an extreme SLCF, the question of the quantitative effect of O₃ on the climate impact of study site over a time horizon of 100 years cannot be answered unambiguously. Tropospheric O₃ is an important greenhouse gas (Myhre et al., 2013). If there are no changes both of the ozone production from its precursors and of the deposition rate, the long-term O₃ concentration would remain constant. The IPCC emission scenarios (Collins et al., 2013) show that only in the most optimistic case (RCP 2.6) does the future O₃ concentration decrease in Europe. In all other RCPs, O₃ will remain at current levels or even increase (Eyring et al., 2013). In the case of rising O₃ background concentrations, the O₃ deposition flux would also increase. Additionally, with rising air temperature and a longer growing season due to global warming, stomatal O₃ uptake could occur over a longer period within a year (Anav et al., 2019; Hayes et al., 2019). In consequence, both effects might lead to an increased deposition rate, implicating a cooling effect on climate. At the same time, an increasing O₃ background concentration might also cause structural and physiological plant damage (Rinnan, 2004), which could reduce C uptake by gross primary production (Oliver et al., 2018) and lower CH₄ emissions through plant-mediated/aerenchymatous transport. Note that the effective impact of increased O₃ background concentration on CO₂ and CH₄ fluxes in peatland ecosystems has rarely been estimated and could be rather small (Haapala et al., 2011; Toet et al., 2017; Williamson et al., 2016).

A comparison of the hypothetical O₃ balance before with the measured O₃ balance 18 years after rewetting remains challenging as studies of ozone deposition over baer (degraded) peat soil still do not exist (Clifton et al., 2020). We may postulate that the site just consisted of baer soil without plants before restoration. In this case there is neither stomatal deposition nor cuticular uptake, and deposition to the baer soil remains as the only O₃ sink. This might lead to a somewhat smaller v_d and F_{O_3} before restoration. However, it is known that v_d without vegetation is not necessarily less than with vegetation (Stella, Loubet, et al., 2011; Stella et al., 2013), and thus the difference in F_{O_3} before and after restoration could be rather small or even negligible.

4. Conclusions

Fluxes of the five most important GHG were measured at a rewetted cut-over raised bog in NW Germany, 18 years after rewetting. Summing up the annual emissions of CO₂, CH₄, and N₂O in 2017 yields a balance of $+500 \pm 120$ g CO₂-equiv m⁻² a⁻¹. With a probability approaching 100%, the site was still a source of GHG in terms of CO₂-equivalents over a SGWP time horizon of 100 years. We suggest that the site is still in the first phase after rewetting, during which CH₄ emissions rise. Based on the finding of an increasing abundance of *Sphagnum spp.* within the dominating aerenchymatous plant species, we hypothesize that the site will turn to a sink within the next two decades. The deposition flux of O₃ has a cooling effect of -77 ± 19 g CO₂-equiv m⁻² a⁻¹, yielding a still positive balance of $+430 \pm 120$ g CO₂-equiv m⁻² a⁻¹.

All balances reported in our study are based on the SGWP approach, while most studies in the past are based on the traditional GWP approach. To complete the picture, we might assume the traditional $GW P_{100}^{CH_4} = 27.2$ (non-fossil) and $GW P_{100}^{N_2O} = 273$ (Forster et al., 2021). Then CH₄ contributed $+237 \pm 75$ g CO₂-equiv m⁻² a⁻¹, while the annual contribution of N₂O was $+38 \pm 20$ g CO₂-equiv m⁻² a⁻¹, which yields a GWP (100 years) balance of $+347 \pm 78$ g CO₂-equiv m⁻² a⁻¹ for CO₂, CH₄, and N₂O in 2017.

Finally, 18 years after rewetting and assuming a zero baseline, the site is still a source of greenhouse gases, regardless of the choice of either the GWP or the SGWP approach. The deposition of near-surface O₃ adds a cooling effect. We estimated the impact of this contribution based on the SGWP metric. Note that there are shortcomings of the SGWP metric when it comes to the inclusion of short-lived greenhouse gases (SLCF) into an overall balance.

We trust that that we used the best possible approach to include SLCF gases such as O₃. To our knowledge, this is the first time that the annual O₃ deposition flux was obtained at a rewetted raised bog ecosystem.

In the perspective of a future increasing O₃ background concentration, another research topic arises: an increased stomatal uptake of O₃ leads to structural and physiological damage of the vegetation. This might cause a decrease in the uptake of CO₂, but also a decrease of the emissions of CH₄. We refrain from speculating of the combination of these effects may lead to a net cooling or net warming impact on the global atmosphere.

In our study, a response of the CH₄ flux to changes in the water level was not observed. A general process-based investigation of possible covariables driving the observed fluxes will be presented in a follow-up study, which will further include additional CO₂, CH₄, and H₂O fluxes from a second site nearby.

We emphasize that our study was based on the assumption of a zero baseline, that is, a comparison between our rewetted peatland and an area with zero emissions. This is a widely used approach, and thus makes our results comparable to GHG balance studies from other peatlands and ecosystems. However, the question arises of how the properties of any alternative scenario may be alike: What would the situation be alike if the area had not been rewetted? A comparison with the (IPCC, 2014) emission factor reveals that our yearly emissions from the rewetted site are lower than those of a temperate peatland recently drained for peat extraction (Section 3.6.1). Note that this comparison is nothing more than a rough estimate. In order to obtain reliable and high-quality data for such a comparison, future studies should conduct simultaneous flux measurements in one peatland at both a rewetted area and an area still under peat harvesting. Then it will be possible to balance flux differences occurring due to land use while not being affected by other effects such as local climate or weather.

For policy makers: First, 18 years after restoration, the peatland is still releasing more GHG than it takes up, which makes it a GHG source. Nonetheless, it is likely that the yearly emissions are already lower than they would have been if restoration had not started 18 years ago. Secondly, based on the positive development of the vegetation, including mosses, we hypothesize that the annual emissions will continue decreasing over the next decades. The rewetting of the site was a good decision in 1999, which helps to mitigate global warming and to reduce the local carbon footprint today.

Acknowledgments

We are deeply indebted to many persons and institutions who made this research possible. Geerd Smidt of the Europäisches Fachzentrum Moor und Klima helped to identify a suitable bog for our studies. The Torf- und Humuswerk Uchte GmbH, represented by Manfred Bischoff and Reinhold Radtke, provided access and logistic support during the experimental phase. The nature conservation authority of the district of Nienburg (Weser) provided the legal permits for this project. We gratefully acknowledge the German federal state of Lower Saxony for providing ozone data from Lufthygienisches Überwachungssystem Niedersachsen. Additionally, we thank numerous persons for their assistance during our fieldwork, among them Lisa Bartsch, Jana Bölter, Elisa Braechevelt, Bettina Breuer, Michael Cormann, Laura Ehrnsperger, Maximilian Küper, Hanna Lokys, Carmen Loschke, Christian Peitzmeier, Elena Plank, Petra Steffen, Peter Sulmann, Weiti Tseng, Hanna Wiedenhaus, and Timo Zimmermann. We thank Celeste Brennecke for language-editing of an earlier version of this manuscript. Last not least, we thank the editor, and two anonymous reviewers for their very thoughtful comments on an earlier version of this manuscript. Open Access funding enabled and organized by Projekt DEAL.

Data Availability Statement

The flux data is available on the European Fluxes Database Cluster, site code DE-UtM, <http://www.europe-flux-data.eu/home/site-details?id=DE-UtM>.

References

- Aamaas, B., Peters, G. P., & Fuglestedt, J. S. (2013). Simple emission metrics for climate impacts. *Earth System Dynamics*, 4(1), 145–170. <https://doi.org/10.5194/esd-4-145-2013>
- Alm, J., Shurpali, N. J., Minkinen, K., Aro, L., Hytönen, J., Laurila, T., & Laine, J. (2007). Emission factors and their uncertainty for the exchange of CO₂, CH₄ and N₂O in Finnish managed peatlands. *Boreal Environment Research*, 12, 191–209.
- Anav, A., Marco, A. D., Friedlingstein, P., Savi, F., Sicard, P., Sitch, S., et al. (2019). Growing season extension affects ozone uptake by European forests. *The Science of the Total Environment*, 669, 1043–1052. <https://doi.org/10.1016/j.scitotenv.2019.03.020>
- Andersen, R., Farrell, C., Graf, M., Muller, F., Calvar, E., Frankard, P., et al. (2017). An overview of the progress and challenges of peatland restoration in Western Europe: Peatland restoration in Western Europe. *Restoration Ecology*, 25(2), 271–282. <https://doi.org/10.1111/rec.12415>
- Andersen, R., Francez, A.-J., & Rochefort, L. (2006). The physicochemical and microbiological status of a restored bog in Québec: Identification of relevant criteria to monitor success. *Soil Biology and Biochemistry*, 38(6), 1375–1387. <https://doi.org/10.1016/j.soilbio.2005.10.012>
- Aubinet, M., Grelle, A., Ibrom, A., Rannik, U., Moncrieff, J., Foken, T., & Vesala, T. (2000). Estimates of the annual net carbon and water exchange of forests: The EUROFLUX methodology. *Advances in Ecological Research*, 30(30), 113–175.
- Augustin, J., & Joosten, H. (2007). Peatland rewetting and the greenhouse effect. *International Mire Conservation Group Newsletter*, (3), 29–30.
- Bacon, K., Baird, A., Blundell, A., Bourgault, M.-A., Chapman, P., Dargie, G., & Young, D. (2017). Questioning ten common assumptions about peatlands. *Mires & Peat*, (19), 1–23. <https://doi.org/10.19189/MaP.2016.OMB.253>
- Bain, C., Bonn, A., Stoneman, R., Chapman, S., Coupar, A., Evans, M., & Worrall, F. (2011). *IUCN UK Commission of inquiry on peatlands (Tech. Rep.)*. IUCN UK Peatland Programme.
- Beyer, C., & Höper, H. (2015). Greenhouse gas exchange of rewetted bog peat extraction sites and a Sphagnum cultivation site in northwest Germany. *Biogeosciences*, 12(7), 2101–2117. <https://doi.org/10.5194/bg-12-2101-2015>
- Blodau, C. (2002). Carbon cycling in peatlands: A review of processes and controls. *Environmental Reviews*, 10(2), 111–134. <https://doi.org/10.1139/a02-004>
- Blodau, C., Basiliko, N., & Moore, T. R. (2004). Carbon turnover in peatland mesocosms exposed to different water table levels. *Biogeochemistry*, 67(3), 331–351. <https://doi.org/10.1023/B:Biog.0000015788.30164.E2>
- Brummell, M. E., Lazzano, C., & Strack, M. (2017). The effects of Eriophorum vaginatum on N₂O fluxes at a restored, extracted peatland. *Ecological Engineering*, 106, 287–295. <https://doi.org/10.1016/j.ecoleng.2017.06.006>

- BUND Diepholzer Moorniederung. (2016). "Großes Uchter Moor bei Uchte – ein Hochmoor mit Potential". *Kranichschutz und Kranich erleben III*.
- Clifton, O. E., Fiore, A. M., Massman, W. J., Baublitz, C. B., Coyle, M., Emberson, L., et al. (2020). Dry deposition of ozone over land: Processes, measurement, and modeling. *Reviews of Geophysics*, 58(1). <https://doi.org/10.1029/2019RG000670>
- Collins, M., Knutti, R., Arblaster, J., Dufresne, J.-L., Fichet, T., Friedlingstein, P., & Wehner, M. (2013). Long-term climate change: Projections, commitments and irreversibility [book section]. In T. Stocker(Eds.), *Climate change 2013: The physical science basis. Contribution of working Group I to the fifth assessment report of the intergovernmental panel on climate change*, (pp. 1029–1136). Cambridge University Press. <https://doi.org/10.1017/CBO9781107415324.024>
- Cooper, M. D. A., Evans, C. D., Zielinski, P., Levy, P. E., Gray, A., Peacock, M., et al. (2014). (November). Infilled ditches are hotspots of landscape methane flux following peatland Re-wetting. *Ecosystems*, 17(7), 1227–1241. <https://doi.org/10.1007/s10021-014-9791-3>
- Dentener, F., Keating, T., & Akimoto, H. (2010). Hemispheric transport of air pollution 2010: Part A: Ozone and particulate matter, air pollut. *Air Pollution Studies*, 17, 305.
- Detto, M., Verfaillie, J., Anderson, F., Xu, L. K., & Baldocchi, D. (2011). (October)Comparing laser-based open- and closed-path gas analyzers to measure methane fluxes using the eddy covariance method. *Agricultural and Forest Meteorology*, 151(10), 1312–1324. <https://doi.org/10.1016/j.agrformet.2011.05.014>
- Drusch, M., Del Bello, U., Carlier, S., Colin, O., Fernandez, V., Gascon, F., et al. (2012). Sentinel-2: ESA's optical high-resolution mission for GMES operational services. *Remote Sensing of Environment*, 120, 25–36. <https://doi.org/10.1016/j.rse.2011.11.026>
- Ducker, J. A., Holmes, C. D., Keenan, T. F., Fares, S., Goldstein, A. H., Mammarella, I., et al. (2018). Synthetic ozone deposition and stomatal uptake at flux tower sites. *Biogeosciences*, 15(17), 5395–5413. <https://doi.org/10.5194/bg-15-5395-2018>
- El-Madany, T., Niklasch, K., & Klemm, O. (2017). Stomatal and Non-stomatal turbulent deposition flux of ozone to a managed peatland. *Atmosphere*, 8(12), 175. <https://doi.org/10.3390/atmos8090175>
- Emsens, W.-J., van Diggelen, R., Aggenbach, C. J. S., Cajthaml, T., Frouz, J., Klimkowska, A., et al. (2020). Recovery of fen peatland microbiomes and predicted functional profiles after rewetting. *The ISME Journal*, 14(7), 1701–1712. <https://doi.org/10.1038/s41396-020-0639-x>
- Erismann, J. W., Van Pul, A., & Wyers, P. (1994). Parametrization of surface resistance for the quantification of atmospheric deposition of acidifying pollutants and ozone. *Atmospheric Environment*, 28(16), 2595–2607. [https://doi.org/10.1016/1352-2310\(94\)90433-2](https://doi.org/10.1016/1352-2310(94)90433-2)
- Eyring, V., Arblaster, J. M., Cionni, I., Sedláček, J., Perlwitz, J., Young, P. J., et al. (2013). Long-term ozone changes and associated climate impacts in CMIP5 simulations: Ozone and associated climate impacts. *Journal of Geophysical Research: Atmospheres*, 118, 5029–5060. <https://doi.org/10.1002/jgrd.50316>
- Falge, E., Baldocchi, D., Olson, R., Anthoni, P., Aubinet, M., Bernhofer, C., et al. (2001). Gap filling strategies for defensible annual sums of net ecosystem exchange. *Agricultural and Forest Meteorology*, 107(1), 43–69. [https://doi.org/10.1016/s0168-1923\(00\)00225-2](https://doi.org/10.1016/s0168-1923(00)00225-2)
- Finkelstein, P. L., & Sims, P. F. (2001). Sampling error in eddy correlation flux measurements. *Journal of Geophysical Research*, 106(D4), 3503–3509. <https://doi.org/10.1029/2000jd900731>
- Foken, T., Göckede, M., Mauder, M., Mahr, L., Amiro, B., & Munger, J. (2004). Post-field data quality control. In X. Lee, W. Massman, & B. Law (Eds.), *Handbook of Micrometeorology: A guide for surface flux measurement and analysis*, (pp. 181–208). Kluwer Academic Publishers.
- Forster, P., Storelvmo, T., Armour, K., Collins, W., Dufresne, J.-L., Frame, D., & Zhang, H. (2021). Anthropogenic and natural radiative forcing. In V. Masson-Delmotte, P. Zhai, A. Pirani, S. L. Connors, C. Peán, S. Berger, et al. (Eds.), *Climate change 2021: The physical science basis. Contribution of working group I to the sixth assessment report of the intergovernmental panel on climate change*. Cambridge University Press.
- Fratini, G., & Mauder, M. (2014). Towards a consistent eddy-covariance processing: An intercomparison of EddyPro and TK3. *Atmospheric Measurement Techniques*, 7(7), 2273–2281. <https://doi.org/10.5194/amt-7-2273-2014>
- Frolking, S., & Roulet, N. T. (2007). Holocene radiative forcing impact of northern peatland carbon accumulation and methane emissions. *Global Change Biology*, 13(5), 1079–1088. <https://doi.org/10.1111/j.1365-2486.2007.01339.x>
- Fuglestad, J., Shine, K., Bernsten, T., Cook, J., Lee, D., Stenke, A., et al. (2010). Transport impacts on atmosphere and climate: Metrics. *Atmospheric Environment*, 44(37), 4648–4677. <https://doi.org/10.1016/j.atmosenv.2009.04.044>
- Fuhrer, J., & Booker, F. (2003). Ecological issues related to ozone: Agricultural issues. *Environment International*, 29(2–3), 141–154. [https://doi.org/10.1016/S0160-4120\(02\)00157-5](https://doi.org/10.1016/S0160-4120(02)00157-5)
- Galbally, I. E., & Roy, C. R. (1980). Destruction of ozone at the earth's surface. *Quarterly Journal of the Royal Meteorological Society*, 106(449), 599–620. <https://doi.org/10.1002/qj.49710644915>
- Goldberg, D. L., Vinciguerra, T. P., Hosley, K. M., Loughner, C. P., Canty, T. P., Salawitch, R. J., & Dickerson, R. R. (2015). Evidence for an increase in the ozone photochemical lifetime in the eastern United States using a regional air quality model: Increasing region of influence on ozone. *Journal of Geophysical Research: Atmospheres*, 120, 12778–12793. <https://doi.org/10.1002/2015JD023930>
- Gorham, E. (1991). Northern peatlands: Role in the carbon cycle and probable responses to climatic warming. *Ecological Applications*, 1(2), 182–195. <https://doi.org/10.2307/1941811>
- Gray, A., Levy, P. E., Cooper, M. D. A., Jones, T., Gaiawyn, J., Leeson, S. R., et al. (2013). Methane indicator values for peatlands: A comparison of species and functional groups. *Global Change Biology*, 19(4), 1141–1150. <https://doi.org/10.1111/gcb.12120>
- Greenup, A. L., Bradford, M. A., McNamara, N. P., Ineson, P., & Lee, J. A. (2000). The role of Eriophorum vaginatum in CH₄ flux from an ombrotrophic peatland. *Plant and Soil*, 227, 265–272. <https://doi.org/10.1023/A:1026573727311>
- Guidi, L., Nali, C., Lorenzini, G., Filippi, F., & Soldatini, G. F. (2001). Effect of chronic ozone fumigation on the photosynthetic process of poplar clones showing different sensitivity. *Environmental Pollution*, 10. [https://doi.org/10.1016/s0269-7491\(00\)00194-9](https://doi.org/10.1016/s0269-7491(00)00194-9)
- Haapala, J. K., Mörsky, S. K., Rinnan, R., Saarnio, S., Martikainen, P. J., Holopainen, T., & Silvola, J. (2011). Long-term effects of ozone on CO₂ exchange in peatland microcosms. *Atmospheric Environment*, 45(24), 4002–4007. <https://doi.org/10.1016/j.atmosenv.2011.04.057>
- Harpenslager, S. F., van den Elzen, E., Kox, M. A., Smolders, A. J., Ettwig, K. F., & Lamers, L. P. (2015). Rewetting former agricultural peatlands: Topsoil removal as a prerequisite to avoid strong nutrient and greenhouse gas emissions. *Ecological Engineering*, 84, 159–168. <https://doi.org/10.1016/j.ecoleng.2015.08.002>
- Hayes, F., Mills, G., Alonso, R., González-Fernández, I., Coyle, M., Grünhage, L., & Marzuoli, R. (2019). A site-specific analysis of the implications of a changing ozone profile and climate for stomatal ozone fluxes in Europe. *Water, Air, & Soil Pollution*, 230(1). <https://doi.org/10.1007/s11270-018-4057-x>
- Helbig, M., Waddington, J. M., Alekseychik, P., Amiro, B., Aurela, M., Barr, A. G., et al. (2020). The biophysical climate mitigation potential of boreal peatlands during the growing season. *Environmental Research Letters*, 15(10), 104004. <https://doi.org/10.1088/1748-9326/abab34>
- Höper, H., Augustin, J., Cagampan, J., Drösler, M., Lundin, L., Moors, E., & Wilson, D. (2008). Restoration of peatlands and greenhouse gas balances. In M. Strack (Ed.), *Peatlands and climate change. Jyväskylä, Finland*. International Peat Society.
- Huth, V., Günther, A., Bartel, A., Gutekunst, C., Heinze, S., Hofer, B., et al. (2021). The climate benefits of topsoil removal and Sphagnum introduction in raised bog restoration. *Restoration Ecology*. <https://doi.org/10.1111/rec.13490>

- Ibrom, A., Dellwik, E., Flyvbjerg, H., Jensen, N. O., & Pilegaard, K. (2007). Strong low-pass filtering effects on water vapour flux measurements with closed-path eddy correlation systems. *Agricultural and Forest Meteorology*, *147*(3–4), 140–156. <https://doi.org/10.1016/j.agrformet.2007.07.007>
- Ibrom, A., Dellwik, E., Larsen, S. E., & Pilegaard, K. (2007). On the use of the Webb–Pearman–Leuning theory for closed-path eddy correlation measurements. *Tellus B: Chemical and Physical Meteorology*, *59*(5), 937–946. <https://doi.org/10.1111/j.1600-0889.2007.00311.x>
- Iglesias-Suarez, F., Kinnison, D. E., Rap, A., Maycock, A. C., Wild, O., & Young, P. J. (2018). Key drivers of ozone change and its radiative forcing over the 21st century. *Atmospheric Chemistry and Physics*, *18*(9), 6121–6139. <https://doi.org/10.5194/acp-18-6121-2018>
- Inglett, K. S., Inglett, P. W., Reddy, K. R., & Osborne, T. Z. (2012). Temperature sensitivity of greenhouse gas production in wetland soils of different vegetation. *Biogeochemistry*, *108*(1/3), 77–90. <https://doi.org/10.1007/s10533-011-9573-3>
- IPCC. (2014). In T. Hiraishi, T. Krug, K. Tanabe, N. Srivastava, J. Baasansuren, M. Fukuda & T.G. Troxler (Eds.), *2013 supplement to the 2006 IPCC guidelines for national greenhouse gas inventories: Wetlands*. Intergovernmental Panel on Climate Change.
- Jackowicz-Korczyński, M., Christensen, T. R., Bäckstrand, K., Crill, P., Friborg, T., Mastepanov, M., & Ström, L. (2010). Annual cycle of methane emission from a subarctic peatland. *Journal of Geophysical Research*, *115*, G02009. <https://doi.org/10.1029/2008JG000913>
- Jacob, D. (2000). Heterogeneous chemistry and tropospheric ozone. *Atmospheric Environment*, *34*(12–14), 2131–2159. [https://doi.org/10.1016/S1352-2310\(99\)00462-8](https://doi.org/10.1016/S1352-2310(99)00462-8)
- Järveoja, J., Peichl, M., Maddison, M., Soosaar, K., Vellak, K., Karofeld, E., et al. (2016, May). Impact of water table level on annual carbon and greenhouse gas balances of a restored peat extraction area. *Biogeosciences*, *13*(9), 2637–2651. <https://doi.org/10.5194/bg-13-2637-2016>
- Joosten, H. (2010). *The Global Peatland CO2 Picture: Peatland status and drainage related emissions in all countries of the world*. Wetlands International.
- Joosten, H., & Clarke, D. (2002). *Wise use of mires and peatlands: Background and principles including a framework for decision-making*. International Peat Society/International Mire Conservation Group.
- Joosten, H., Tanneberger, F., & Moen, A. (Eds.). (2017). *Mires and peatlands of Europe: Status, distribution and conservation*. Schweizerbart Science Publishers.
- Jordan, S., Strömgren, M., & Fiedler, J. (2016). Ecosystem respiration, methane and nitrous oxide fluxes from ecotopes in a rewetted extracted peatland in Sweden. *Mires & Peat*, *17*(7), 1–23. <https://doi.org/10.19189/Map.2016.OMB.224>
- Kaimal, J. C., & Finnigan, J. J. (1994). *Atmospheric boundary layer flows: Their structure and measurement*. Oxford University Press.
- Kaimal, J. C., Izumi, Y., Wyngaard, J. C., & Coté, O. R. (1972). Spectral characteristics of surface-layer turbulence. *Quarterly Journal of the Royal Meteorological Society*, *98*(417), 563–589. <https://doi.org/10.1002/qj.49709841707>
- Kandel, T. P., Karki, S., Elsgaard, L., & Lærke, P. E. (2019). Fertilizer-induced fluxes dominate annual N2O emissions from a nitrogen-rich temperate fen rewetted for paludiculture. *Nutrient Cycling in Agroecosystems*, *115*(1), 57–67. <https://doi.org/10.1007/s10705-019-10012-5>
- Kivimäki, S. K., Yli-petäys, M., & Tuittila, E.-s. (2007). Carbon sink function of sedge and Sphagnum patches in a restored cut-away peatland: Increased functional diversity leads to higher production: Restoration of cut-away peatland. *Journal of Applied Ecology*, *45*(3), 921–929. <https://doi.org/10.1111/j.1365-2664.2008.01458.x>
- Kljun, N., Calanca, P., Rotach, M. W., & Schmid, H. P. (2015). A simple two-dimensional parameterisation for flux footprint prediction (FFP). *Geoscientific Model Development*, *8*(11), 3695–3713. <https://doi.org/10.5194/gmd-8-3695-2015>
- Komulainen, V.-M., Nykänen, H., Martikainen, P. J., & Laine, J. (1998). Short-term effect of restoration on vegetation change and methane emissions from peatlands drained for forestry in southern Finland. *Canadian Journal of Forest Research*, *28*(3), 402–411. <https://doi.org/10.1139/x98-011>
- Komulainen, V.-M., Tuittila, E.-S., Vasander, H., & Laine, J. (1999). Restoration of drained peatlands in southern Finland: Initial effects on vegetation change and CO₂ balance. *Journal of Applied Ecology*, *36*(5), 634–648. <https://doi.org/10.1046/j.1365-2664.1999.00430.x>
- Kottek, M., Grieser, J., Beck, C., Rudolf, B., & Rubel, F. (2006, June). World Map of the Köppen-Geiger climate classification updated. *Meteorologische Zeitschrift*, *15*(3), 259–263. <https://doi.org/10.1127/0941-2948/2006/0130>
- Lamarque, J.-F., Bond, T. C., Eyring, V., Granier, C., Heil, A., Klimont, Z., et al. (2010). Historical (1850–2000) gridded anthropogenic and biomass burning emissions of reactive gases and aerosols: Methodology and application. *Atmospheric Chemistry and Physics*, *10*(15), 7017–7039. <https://doi.org/10.5194/acp-10-7017-2010>
- Lamaud, E., Loubet, B., Irvine, M., Stella, P., Personne, E., & Cellier, P. (2009). Partitioning of ozone deposition over a developed maize crop between stomatal and non-stomatal uptakes, using eddy-covariance flux measurements and modelling. *Agricultural and Forest Meteorology*, *149*(9), 1385–1396. <https://doi.org/10.1016/j.agrformet.2009.03.017>
- Leifeld, J., & Menichetti, L. (2018). The underappreciated potential of peatlands in global climate change mitigation strategies. *Nature Communications*, *9*(1). <https://doi.org/10.1038/s41467-018-03406-6>
- Louis, J., Debaecker, V., Pflug, B., Main-Knorn, M., Bieniarz, J., Mueller-Wilm, U., & Gascon, F. (2016). *Sentinel-2 SEN2COR: L2A processor for users*. European Space Agency.
- Mathijssen, P. J. H., Kähkölä, N., Tuovinen, J.-P., Lohila, A., Minkkinen, K., Laurila, T., & Väiliranta, M. (2017). Lateral expansion and carbon exchange of a boreal peatland in Finland resulting in 7000 years of positive radiative forcing: PEAT SUCCESSION, C FLUX, AND CLIMATE FORCING. *Journal of Geophysical Research: Biogeosciences*, *122*, 562–577. <https://doi.org/10.1002/2016JG003749>
- Mauder, M., Cuntz, M., Drue, C., Graf, A., Rebmann, C., Schmid, H. P., et al. (2013). A strategy for quality and uncertainty assessment of long-term eddy-covariance measurements. *Agricultural and Forest Meteorology*, *169*, 122–135. <https://doi.org/10.1016/j.agrformet.2012.09.006>
- McDermitt, D., Burba, G., Xu, L., Anderson, T., Komissarov, A., Riensche, B., et al. (2011). A new low-power, open-path instrument for measuring methane flux by eddy covariance. *Applied Physics B-Lasers & Optics*, *102*(2), 391–405. <https://doi.org/10.1007/s00340-010-4307-0>
- Moncrieff, J., Clement, R., Finnigan, J., & Meyers, T. (2004). Averaging, detrending, and filtering of eddy covariance time series. In X. Lee, W. J. Massman, & B. E. Law (Eds.), *Handbook of Micrometeorology: A guide for surface flux measurement and analysis* (pp. 7–31). Kluwer Academic Publishers.
- Money, R., & Wheeler, B. (1999). Some critical questions concerning the restorability of damaged raised bogs. *Applied Vegetation Science*, *2*(1), 107–116. <https://doi.org/10.2307/1478887>
- Monks, P. S., Archibald, A. T., Colette, A., Cooper, O., Coyle, M., Derwent, R., et al. (2015). Tropospheric ozone and its precursors from the urban to the global scale from air quality to short-lived climate forcer. *Atmospheric Chemistry and Physics*, *15*(15), 8889–8973. <https://doi.org/10.5194/acp-15-8889-2015>
- Myhre, G., Shindell, D., Bréon, F.-M., Collins, W., Fuglestedt, J., Huang, J., & Zhang, H. (2013). Anthropogenic and natural radiative forcing [book section] In T. Stocker (Eds.), *Climate change 2013: The physical science basis. Contribution of working group I to the fifth assessment report of the intergovernmental panel on climate change* (pp. 659–740). Cambridge University Press. <https://doi.org/10.1017/CBO9781107415324.018>
- Neubauer, S. C., & Megonigal, J. P. (2015). Moving beyond global warming potentials to quantify the climatic role of ecosystems. *Ecosystems*, *18*(6), 1000–1013. <https://doi.org/10.1007/s10021-015-9879-4>

- Neubauer, S. C., & Megonigal, J. P. (2019). Correction to: Moving beyond global warming potentials to quantify the climatic role of ecosystems. *Ecosystems*, 22(8), 1931–1932. <https://doi.org/10.1007/s10021-019-00422-5>
- Nijp, J. J., Limpens, J., Metselaar, K., Peichl, M., Nilsson, M. B., van der Zee, S. E. A. T. M., & Berendse, F. (2015). Rain events decrease boreal peatland net CO₂ uptake through reduced light availability. *Global Change Biology*, 21(6), 2309–2320. <https://doi.org/10.1111/gcb.12864>
- Oliver, R. J., Mercado, L. M., Sitch, S., Simpson, D., Medlyn, B. E., Lin, Y.-S., & Folberth, G. A. (2018). Large but decreasing effect of ozone on the European carbon sink. *Biogeosciences*, 15(13), 4245–4269. <https://doi.org/10.5194/bg-15-4245-2018>
- Page, S., & Baird, A. (2016). Peatlands and global change: Response and Resilience. *Annual Review of Environment and Resources*, 41(1), 35–57. <https://doi.org/10.1146/annurev-environ-110615-085520>
- Papale, D., Reichstein, M., Aubinet, M., Canfora, E., Bernhofer, C., Kutsch, W., et al. (2006). Towards a standardized processing of Net Ecosystem Exchange measured with eddy covariance technique: Algorithms and uncertainty estimation. *Biogeosciences*, 3(4), 571–583. <https://doi.org/10.5194/bg-3-571-2006>
- Pierrehumbert, R. (2014). Short-lived climate pollution. *Annual Review of Earth and Planetary Sciences*, 42(1), 341–379. <https://doi.org/10.1146/annurev-earth-060313-054843>
- Putkinen, A., Tuittila, E.-S., Siljanen, H. M., Bodrossy, L., & Fritze, H. (2018). Recovery of methane turnover and the associated microbial communities in restored cutover peatlands is strongly linked with increasing Sphagnum abundance. *Soil Biology and Biochemistry*, 116, 110–119. <https://doi.org/10.1016/j.soilbio.2017.10.005>
- R Core Team. (2017). *R: A language and environment for statistical computing*. R Foundation for Statistical Computing.
- Ramsar Sites Information Service. (1976). *Site 86, diepholzer Moorniederung*. Retrieved from <https://rsis.ramsar.org/ris/86>
- Reichstein, M., Falge, E., Baldocchi, D., Papale, D., Aubinet, M., Berbigier, P., et al. (2005). On the separation of net ecosystem exchange into assimilation and ecosystem respiration: Review and improved algorithm. *Global Change Biology*, 11(9), 1424–1439. <https://doi.org/10.1111/j.1365-2486.2005.001002.x>
- Richard, K. (1990). Torfgewinnung und Torfverwertung. In K. Göttlich (Ed.), *Moor- und Torfkunde* (3rd ed., pp. 411–472). E. Schweizerbart'sche Verlagsbuchhandlung (Nägele u. Obermiller).
- Rinnan, R. (2004). Ozone effects on the ultrastructure of peatland plants: Sphagnum mosses, vaccinium oxycoccus, andromeda polifolia and Eriophorum vaginatum. *Annals of Botany*, 94(4), 623–634. <https://doi.org/10.1093/aob/mch182>
- Rinne, J., Riutta, T., Pihlatie, M., Aurela, M., Haapanala, S., Tuovinen, J. P., et al. (2007). Annual cycle of methane emission from a boreal fen measured by the eddy covariance technique. *Tellus Series B Chemical and Physical Meteorology*, 59(3), 449–457. <https://doi.org/10.1111/j.1600-0889.2007.00261.x>
- Schmidt, G. A., Ruedy, R. A., Miller, R. L., & Lacis, A. A. (2010). Attribution of the present-day total greenhouse effect. *Journal of Geophysical Research*, 115, D20106. <https://doi.org/10.1029/2010JD014287>
- Schneekloth, H., & Schneider, S. (1970). Die Moore in Niedersachsen. 1. Teil: Bereich des Blattes Hannover der Geologischen Karte der Bundesrepublik Deutschland. *Veröffentlichungen des niedersächsischen Instituts für Landeskunde und Landesentwicklung*, 96(1), 1–8.
- Sherwood, S. C., Dixit, V., & Salomez, C. (2018). The global warming potential of near-surface emitted water vapour. *Environmental Research Letters*, 13(10), 104006. <https://doi.org/10.1088/1748-9326/aae018>
- Speyer, E. (2012). Die Torfindustrie in Niedersachsen – Ergebnisse einer Umfrage zur Zukunft der Torfgewinnung in Niedersachsen. *Telma*, 42, 27–42. <https://doi.org/10.23689/fidgeo-2959>
- Stella, P., Loubet, B., Lamaud, E., Laville, P., & Cellier, P. (2011). June). Ozone deposition onto bare soil: A new parameterisation. *Agricultural and Forest Meteorology*, 151(6), 669–681. <https://doi.org/10.1016/j.agrformet.2011.01.015>
- Stella, P., Personne, E., Lamaud, E., Loubet, B., Trebs, I., & Cellier, P. (2013). Assessment of the total, stomatal, cuticular, and soil 2 year ozone budgets of an agricultural field with winter wheat and maize crops. *Journal of Geophysical Research: Biogeosciences*, 118, 1120–1132. <https://doi.org/10.1002/jgrg.20094>
- Stella, P., Personne, E., Loubet, B., Lamaud, E., Ceschia, E., Béziat, P., et al. (2011). Predicting and partitioning ozone fluxes to maize crops from sowing to harvest: The SurfAtm-O₃ model. *Biogeosciences*, 8(10), 2869–2886. <https://doi.org/10.5194/bg-8-2869-2011>
- Ström, L., Mastepanov, M., & Christensen, T. R. (2005). Species-specific effects of vascular plants on carbon turnover and methane emissions from wetlands. *Biogeochemistry*, 75(1), 65–82. <https://doi.org/10.1007/s10533-004-6124-1>
- Swenson, M. M., Regan, S., Bremmers, D. T. H., Lawless, J., Saunders, M., & Gill, L. W. (2019). Carbon balance of a restored and cutover raised bog: Implications for restoration and comparison to global trends. *Biogeosciences*, 16(3), 713–731. <https://doi.org/10.5194/bg-16-713-2019>
- Tanneberger, F., Tegetmeyer, C., Busse, S., Barthelmes, A., Shumka, S., Marine, A. M., & Joosten, H. (2017). The peatland map of Europe. *Mires & Peat*, 19. <https://doi.org/10.19189/Map.2016.OMB.264>
- Taylor, J. R. (1997). *An introduction to error analysis: The study of uncertainties in physical measurements* (2nd ed.). University Science Books.
- Teklemariam, T., Lafleur, P., Moore, T., Roulet, N., & Humphreys, E. (2010). October) The direct and indirect effects of inter-annual meteorological variability on ecosystem carbon dioxide exchange at a temperate ombrotrophic bog. *Agricultural and Forest Meteorology*, 150(11), 1402–1411. <https://doi.org/10.1016/j.agrformet.2010.07.002>
- Toet, S., Oliver, V., Ineson, P., McLoughlin, S., Helgason, T., Peacock, S., et al. (2017). How does elevated ozone reduce methane emissions from peatlands? *The Science of the Total Environment*, 579, 60–71. <https://doi.org/10.1016/j.scitotenv.2016.10.188>
- Tuckett, R. P. (2016). The role of atmospheric gases. In T. M. Letcher (Ed.), *Climate change: Observed impacts on planet Earth* (2nd ed., pp. 375–397). Elsevier. <https://doi.org/10.1016/B978-0-444-63524-2.00024-5>
- Tuittila, E.-S., Komulainen, V.-M., Vasander, H., & Laine, J. (1999). Restored cut-away peatland as a sink for atmospheric CO₂. *Oecologia*, 120(4), 563–574. <https://doi.org/10.1007/s004420050891>
- Tuittila, E.-S., Komulainen, V.-M., Vasander, H., Nykänen, H., Martikainen, P. J., & Laine, J. (2000). Methane dynamics of a restored cut-away peatland. *Global Change Biology*, 6(5), 569–581. <https://doi.org/10.1046/j.1365-2486.2000.00341.x>
- Vanselow-Algan, M., Schmidt, S. R., Greven, M., Fiencke, C., Kutzbach, L., & Pfeiffer, E.-M. (2015). High methane emissions dominated annual greenhouse gas balances 30 years after bog rewetting. *Biogeosciences*, 12(14), 4361–4371. <https://doi.org/10.5194/bg-12-4361-2015>
- Waddington, J. M., & Day, S. M. (2007). Methane emissions from a peatland following restoration. *Journal of Geophysical Research*, 112, G03018. <https://doi.org/10.1029/2007JG000400>
- Waddington, J. M., Strack, M., & Greenwood, M. J. (2010). Toward restoring the net carbon sink function of degraded peatlands: Short-term response in CO₂ exchange to ecosystem-scale restoration. *Journal of Geophysical Research*, 115, G01008. <https://doi.org/10.1029/2009JG001090>
- Webb, E. K., Pearman, G. I., & Leuning, R. (1980). Correction of flux measurements for density effects due to heat and water vapour transfer. *Quarterly Journal of the Royal Meteorological Society*, 106(447), 85–100. <https://doi.org/10.1002/qj.49710644707>
- Weiss, M., & Baret, F. (2016). *S2ToolBox level 2 products: LAI, FAPA, FCOVER*. European Space Agency.
- Wesely, M. (1989). Parameterization of surface resistances to gaseous dry deposition in regional-scale numerical models. *Atmospheric Environment*, 23(6), 1293–1304. [https://doi.org/10.1016/0004-6981\(89\)90153-4](https://doi.org/10.1016/0004-6981(89)90153-4)

- Wesely, M. L., & Hicks, B. B. (2000). A review of the current status of knowledge on dry deposition. *Atmospheric Environment*, *34*(12–14), 2261–2282. [https://doi.org/10.1016/S1352-2310\(99\)00467-7](https://doi.org/10.1016/S1352-2310(99)00467-7)
- Whalen, S. C. (2005). Biogeochemistry of methane exchange between natural wetlands and the atmosphere. *Environmental Engineering Science*, *22*(1), 73–94. <https://doi.org/10.1089/ees.2005.22.73>
- Williamson, J. L., Mills, G., Hayes, F., Jones, T., & Freeman, C. (2016). How do increasing background concentrations of tropospheric ozone affect peatland plant growth and carbon gas exchange? *Atmospheric Environment*, *127*, 133–138. <https://doi.org/10.1016/j.atmosenv.2015.12.004>
- Wilson, D., Alm, J., Laine, J., Byrne, K. A., Farrell, E. P., & Tuittila, E. S. (2009). Rewetting of cutaway peatlands: Are we Re-creating hot spots of methane emissions? *Restoration Ecology*, *17*(6), 796–806. <https://doi.org/10.1111/j.1526-100X.2008.00416.x>
- Wilson, D., Blain, D., & Couwenberg, J. (2016). Greenhouse gas emission factors associated with rewetting of organic soils. *Mires & Peat*, *17*(4), 1–28. <https://doi.org/10.19189/MaP.2016.OMB.222>
- Wilson, D., Farrell, C., Mueller, C., Hepp, S., & Renou-Wilson, F. (2013). Rewetted industrial cutaway peatlands in western Ireland: A prime location for climate change mitigation? *Mires & Peat*, *11*(1), 1–22. <https://doi.org/10.1080/00750778.2013.848542>
- Wilson, D., Farrell, C. A., Fallon, D., Moser, G., Müller, C., & Renou-Wilson, F. (2016). Multiyear greenhouse gas balances at a rewetted temperate peatland. *Global Change Biology*, *22*(12), 4080–4095. <https://doi.org/10.1111/gcb.13325>
- Wilson, D., Tuittila, E.-S., Alm, J., Laine, J., Farrell, E. P., & Byrne, K. A. (2007). Carbon dioxide dynamics of a restored maritime peatland. *Ecoscience*, *14*(1), 712–780. [https://doi.org/10.2980/1195-6860\(2007\)14\[71:cddoar\]2.0.co;2](https://doi.org/10.2980/1195-6860(2007)14[71:cddoar]2.0.co;2)
- Wutzler, T., Lucas-Moffat, A., Migliavacca, M., Knauer, J., Sickel, K., Šigut, L., et al. (2018). Basic and extensible post-processing of eddy covariance flux data with REddyProc. *Biogeosciences*, *15*(16), 5015–5030. <https://doi.org/10.5194/bg-15-5015-2018>
- Wutzler, T., Reichstein, M., Moffat, A. M., & Migliavacca, M. (2018). *REddyProc: Post processing of (Half-) Hourly Eddy-covariance measurements*.
- Young, P. J., Archibald, A. T., Bowman, K. W., Lamarque, J.-F., Naik, V., Stevenson, D. S., et al. (2013). Pre-industrial to end 21st century projections of tropospheric ozone from the atmospheric chemistry and climate model intercomparison project (ACCMIP). *Atmospheric Chemistry and Physics*, *13*(4), 2063–2090. <https://doi.org/10.5194/acp-13-2063-2013>
- Zhang, L., Brook, J. R., & Vet, R. (2002). On ozone dry deposition—With emphasis on non-stomatal uptake and wet canopies. *Atmospheric Environment*, *36*(30), 4787–4799. [https://doi.org/10.1016/S1352-2310\(02\)00567-8](https://doi.org/10.1016/S1352-2310(02)00567-8)
- Zhang, L., Brook, J. R., & Vet, R. (2003). A revised parameterization for gaseous dry deposition in air-quality models. *Atmospheric Chemistry and Physics*, *16*. <https://doi.org/10.5194/acp-3-2067-2003>
- Zhong, Y., Jiang, M., & Middleton, B. A. (2020). Effects of water level alteration on carbon cycling in peatlands. *Ecosystem Health and Sustainability*, *6*(1), 1806113. <https://doi.org/10.1080/20964129.2020.1806113>